Combinatorial Descriptions of the m-Cambrian Lattices

by

Mike Freeze

Bachelor of Science, UNB, 2012

A THESIS SUBMITTED IN PARTIAL FULFILLMENT OF THE REQUIREMENTS FOR THE DEGREE OF

Master's of Science

In the Graduate Academic Unit of Mathematics

Supervisor(s):	Hugh Thomas, PhD, Mathematics
	Barry Monson, PhD, Mathematics
Examining Board:	Colin Ingalls, PhD, Mathematics
	Alyssa Sankey, PhD, Mathematics
	Dennis Tokaryk, PhD, Physics, UNB

This thesis is accepted by the

Dean of Graduate Studies

THE UNIVERSITY OF NEW BRUNSWICK

April, 2016

Abstract

The main object of interest in this thesis is the linear type A_{n-1} family of m-Cambrian lattices. I will provide two concrete combinatorial descriptions of the m-Cambrian lattices, and prove that they are equivalent.

Dedication

For Hana, whose infinite patience and support made this work possible.

Preface

In recent research on cluster algebras, Christian Stump, Hugh Thomas, and Nathan Williams [12] used braid groups to define a natural poset structure on the facets of generalized cluster complexes. These facets are known to be counted by the Fuss-Catalan numbers. However, the lattice obtained is not the m-Tamari lattice. The family of lattices discovered has been dubbed the *m-Cambrian* lattices, and is the main focus of this thesis.

To build an m-Cambrian lattice, we need three inputs: a Coxeter group W, a Coxeter element $c \in W$, and an integer m. For a given Coxeter group, a change of Coxeter element will result in a different family of m-Cambrian lattices. The family of m-Cambrian lattices we are interested in is obtained from the Coxeter group A_{n-1} and the Coxeter element $c = s_1 s_2 \dots s_{n-1}$. We are interested in this case since for $m = 1$, this family of m-Cambrian lattices reduces to the family of Tamari lattices, a well studied family of lattices with elements counted by the Catalan numbers. So in a sense, we are investigating the family of m-Cambrian lattices that is "closest" to the m-Tamari lattice.

As mentioned in the abstract, I will provide two concrete combinatorial descriptions of the m-Cambrian lattices, and prove that they are equivalent.

In Chapter 1 we begin by introducing the reader to a sequence of numbers called the Catalan numbers. We then introduce some poset terminology so that we can discuss lattices. The first family of lattices discussed is the family of Tamari lattices, whose elements are counted by the Catalan numbers. We introduce another sequence which is a generalization of the Catalan numbers, called the Fuss-Catalan numbers. The Fuss-Catalan numbers count the number of elements in the m-Tamari lattices, a family of lattices generalizing the Tamari lattices. The rest of Chapter 1 is dedicated to familiarizing the reader with Coxeter groups, and in particular the group A_{n-1}.

In Chapter 2 we discuss a few important objects which are counted by the Fuss-Catalan numbers. The first objects we discuss are the facets of m-cluster complexes. We generalize the Coxeter group A_{n-1} to its corresponding braid group Braid_{n-1}, and find such facets of m-cluster complexes by searching for reduced expressions of an element in Braid_{n-1} related to the longest element in A_{n-1}. The next Fuss-Catalan objects we discuss are $(m+2)$-angulations of an $(mn+2)$-gon. We can arrange the diagonals in such an angulation into diagrams similar to those drawn for the facets of m-cluster complexes. We then introduce dot diagrams, which are in bijection with both the facets of m-cluster complexes and $(m+2)$-angulations of an

$(mn+2)$-gon. For our purposes, we can think of these dot diagrams as an abstract way of looking at angulations.

In Chapter 3 we introduce two different partial orders on the set of dot diagrams. The family of lattices obtained from both of these partial orders is the family of m-Cambrian lattices of the type we are interested in. Namely, the family of m-Cambrian lattices obtained from the group A_{n-1} and Coxeter element $c = s_1 s_2 \dots s_{n-1}$. The first order we consider is called the rotation order. We describe this order in terms of dot diagrams, and then translate this into a description in terms of angulations. The description in terms of angulations turns out to be a natural generalization of the description of the Tamari lattices in terms of angulations. The second partial order that we consider is called the inclusion order, and is only described in terms of dot diagrams. The main result of the thesis is a proof at the end of the chapter showing that the rotation order and inclusion order are equivalent.

In Chapter 4 we discuss future work which includes proving that these partial orders result in a lattice, finding a description of the inclusion order in terms of angulations, as well as generalizing some other descriptions of the Tamari lattices not discussed in this thesis.

Acknowledgements

I would like to take a moment to sincerely thank the following people, organizations, and institutions:

The Natural Sciences and Engineering Research Council of Canada (NSERC), New Brunswick Innovation Fund (NBIF), University of New Brunswick Mathematics Department, Faculty of Science, and School of Graduate Studies for their generous financial support, travel assistance, as well as organizing many interesting seminars, and conferences over the past two years. Most of all I would like to thank my supervisors Hugh Thomas and Barry Monson for their guidance while helping me to navigate my way through new and interesting areas of mathematics.

Table of Contents

List of Figures

Chapter 1

Introduction

1.1 The Catalan numbers

Few sequences are as pervasive in combinatorial mathematics as the Catalan numbers. This sequence of natural numbers was first studied by Euler while attempting to count the number of ways in which a convex polygon can be divided into triangles. Later work by 17^{th} century French mathematician Eugene Charles Catalan on counting bracketed sequences led him to the same sequence of numbers. The Catalan numbers satisfy the recursive relation

$$C_0 = 1, \quad C_{n+1} = \sum_{i=0}^{n} C_i C_{n-i}, \quad \text{for } n \in \mathbb{N}.$$

In closed form, the n^{th} Catalan number is given by

$$C_n = \frac{1}{n+1}\binom{2n}{n}.$$

We note that the first few Catalan numbers are

$$C_0 = 1, \quad C_1 = 1, \quad C_2 = 2, \quad C_3 = 5, \quad C_4 = 14, \ldots$$

The number C_n counts many objects such as: triangulations of a convex $(n+2)$-gon, bracketed sequences of $n+1$ non-associative variables, Dyck paths of length $2n$, binary trees with n parent nodes, etc. Richard Stanley has compiled a list of over 200 objects that are counted by the Catalan numbers [11].

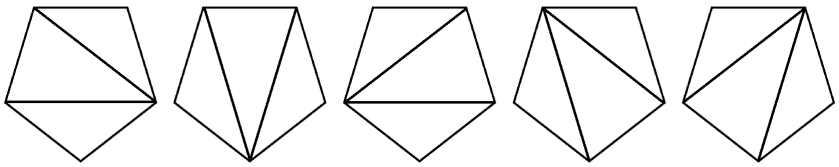

Figure 1.1: The $C_3 = 5$ triangulations of a pentagon.

$$((x_1x_2)x_3)x_4 \quad (x_1(x_2x_3))x_4 \quad (x_1x_2)(x_3x_4) \quad x_1((x_2x_3)x_4) \quad x_1(x_2(x_3x_4))$$

Figure 1.2: The $C_3 = 5$ ways in which we can bracket a set of 4 non-associative variables.

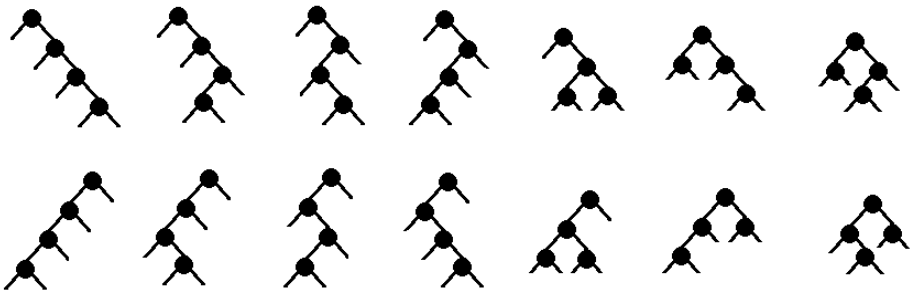

Figure 1.3: The $C_4 = 14$ binary trees with 4 parent nodes.

1.2 The Tamari lattices

1.2.1 Poset terminology

Before we start into the discussion of specific lattices, let us first define what we mean by a lattice in this context.

Definition 1.2.1. *A **poset** $(S, \leq)$ is a finite partially ordered set. That is, the finite set S is equipped with a relation " $\leq$ " which is*

- *reflexive ($x \leq x$ for all $x \in S$),*
- *transitive ($x \leq y$ and $y \leq z$ imply $x \leq z$), and*
- *antisymmetric ($x \leq y$ and $y \leq x$ imply $x = y$).*

We write $x < y$ if $x \leq y$ but $x \neq y$. We say that y *covers* x, written $x \lessdot y$, if $x < y$ and there is no z such that $x < z < y$. The cover relation of a poset is the set of pairs (x, y) with y covering x. It is very useful to have an explicit rule describing when $x \lessdot y$. Often it is helpful to look

at the *Hasse diagram* of a poset $(S, \leq)$. This is a graphical representation of the poset where we draw each element in S as a vertex in the plane, and draw an edge from x up to y if $x \lessdot y$. See Figure 1.4 for an example where $S = \{\{1\}, \{2\}, \{1,3\}, \{1,4\}, \{2,4\}, \{1,2,3,4\}\}$ and the partial ordering is set inclusion.

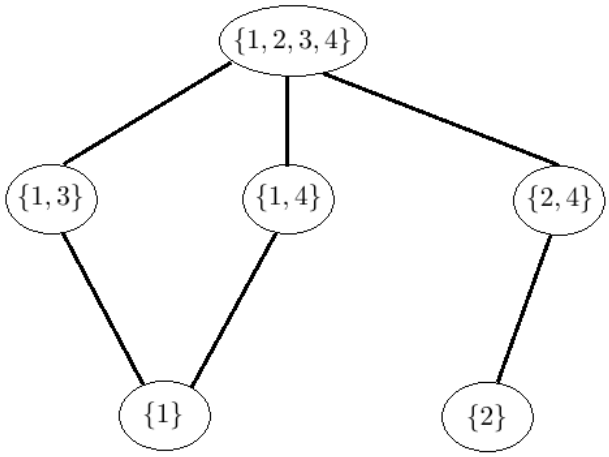

Figure 1.4: An example of a Hasse diagram for a poset.

A poset is *bounded* if it has a unique minimal element $\hat{0}$ and a unique maximal element $\hat{1}$ such that $\hat{0} \leq x \leq \hat{1}$ for all $x \in S$. The poset in Figure 1.4 is not a bounded poset as it does not have a unique minimal element.

Now we are ready to define a lattice.

Definition 1.2.2. *A **lattice** is a bounded poset such that every pair of elements $x, y \in S$ has*

- *a unique minimal upper bound, denoted $x \vee y$ (this is called the join of x and y), and*
- *a unique maximal lower bound, denoted $x \wedge y$ (this is called the meet of x and y).*

See Figure 1.5 for an illustration of the difference between a bounded poset and a lattice. The poset on the left is not a lattice since the elements on the second tier do not have a join (similarly the two elements on the third tier do not have a meet). The poset on the right is a lattice, since each pair of elements has a join and a meet.

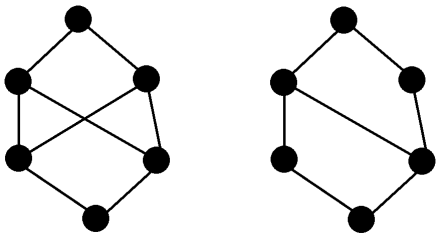

Figure 1.5: Both posets are bounded, but only the one on the right is a lattice.

1.2.2 The Tamari lattices

In the 1950s, German-born mathematician Dov Tamari [13] considered a partial ordering on the set of bracketed sequences of $n + 1$ variables. The resulting poset is T_n, the Tamari lattice with C_n elements. Since its inception, mathematicians have been interested in finding natural realizations of

the Tamari lattices on Catalan objects, along with bijections between these realizations. For example, Bernardi and Bonichon [4] describe bijections between the Tamari lattices on Dyck paths, binary trees, and triangulations of a polygon.

The Hasse diagram of T_n is isomorphic to the 1-skeleton of the $(n-1)$-dimensional associahedron, a well-studied polytope with C_n many vertices [16]. See Figures 1.6 and 1.7 for T_3 and T_4 realized on triangulations of a pentagon and hexagon, respectively. Note that T_3 has $C_3 = 5$ elements, and T_4 has $C_4 = 14$ elements.

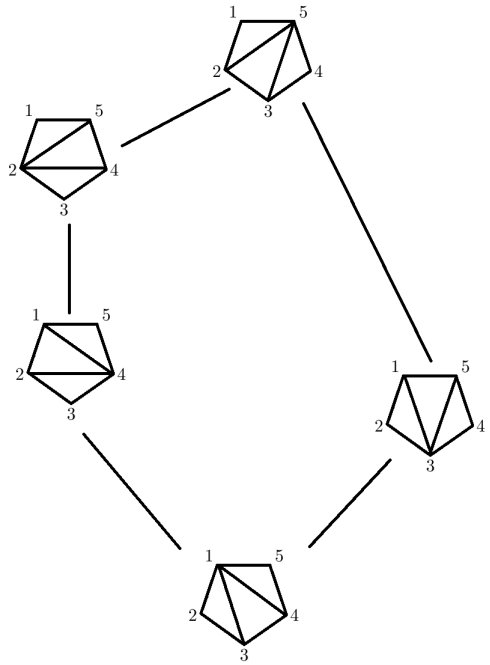

Figure 1.6: The Tamari lattice T_3 realized on triangulations of a pentagon.

We define the cover relations on T_n as follows. Suppose we have

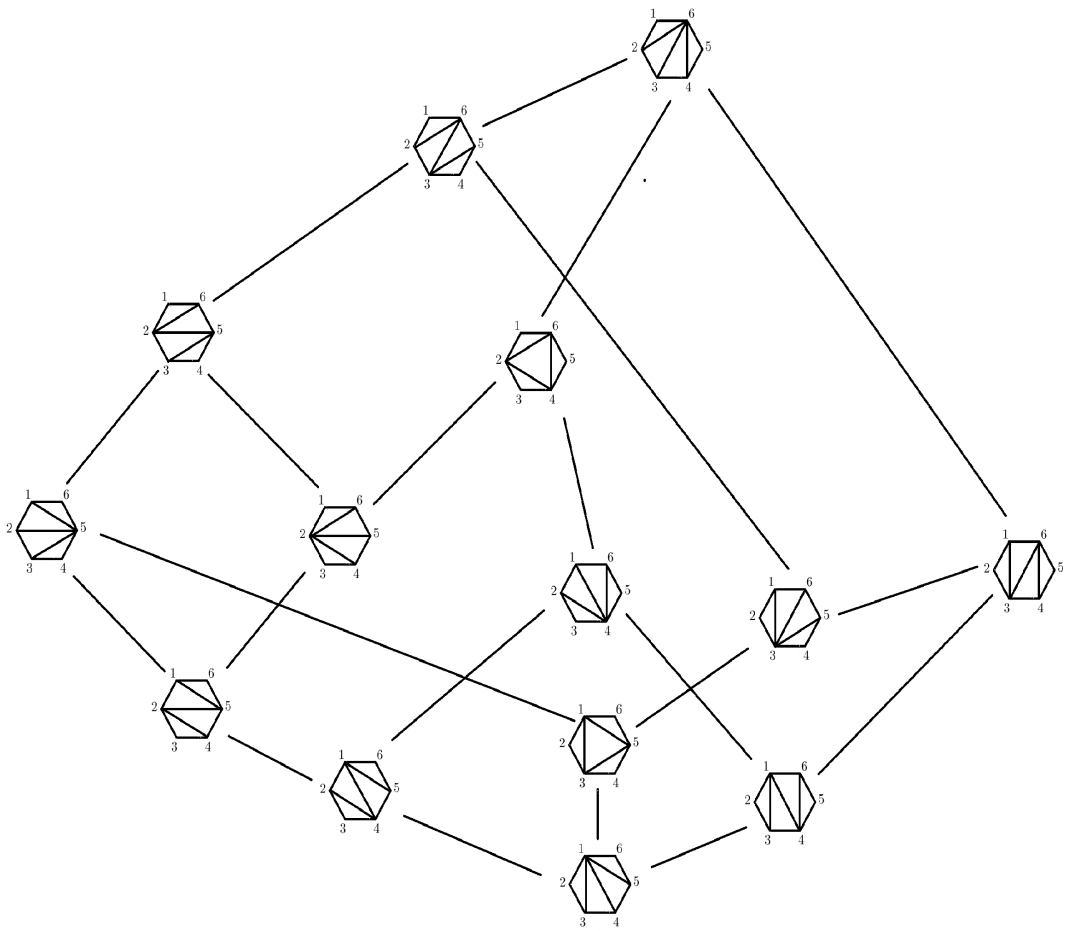

Figure 1.7: The Tamari lattice T_4 realized on triangulations of a hexagon.

two triangulations A and B of an $(n+2)$-gon. Then $A \lessdot B$ if B is obtained from A by flipping a single diagonal such that the vertex labelling increases. That is, if the diagonal (a, b) in A flips to the diagonal (c, d) in B such that $a < c$ and $b < d$, then B covers A. This description requires that we label the vertices of the $(n+2)$-gon in the conventional way, as is the case in Figures 1.6 and 1.7.

Figure 1.8 is inspired by Nathan Reading's chapter from the book *Associahedra, Tamari Lattices and Related Structures* [10]. Reading draws his convex polygons in the following way: draw a horizontal edge. On this edge, label the left vertex 1, and the right vertex $n+2$. The remaining n vertices are arranged so that they lie under the above-mentioned edge, and each vertex $i+1$ lies to the right of vertex i, for $1 \leq i < n+1$. Finish the picture by drawing an edge from vertex i to vertex $i+1$ for each $1 \leq i < n+1$. The advantage to drawing the polygons as Reading does is that the cover relations can be described without referring to a particular vertex labelling. When the polygons are drawn this way, we move up in the lattice by replacing a diagonal in the triangulation with a diagonal of higher slope.

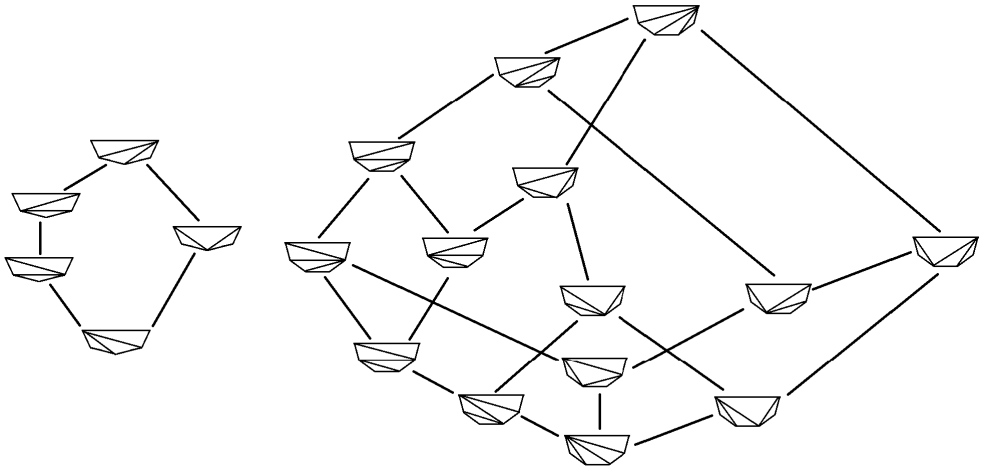

Figure 1.8: The Tamari lattices T_3 (left), and T_4 (right).

1.3 The Fuss-Catalan numbers

The Fuss-Catalan numbers $C_n^{(m)}$, are a generalization of the Catalan numbers with the regular Catalan numbers recovered when $m = 1$. These numbers were discovered circa 1791 by Swiss mathematician Nicolaus Fuss in his attempt to count the number of $(m+2)$-angulations of an $(mn+2)$-gon. The Fuss-Catalan analogues of Catalan objects counted by these numbers include the above-mentioned angulations, $(m+1)$-ary trees with n parent nodes, m-Dyck paths, and so on. The Fuss-Catalan numbers satisfy the recursive relation

$$C_0^{(m)} = 1, \quad C_{n+1}^{(m)} = \sum_{k_1+k_2+\cdots+k_{m+1}=n} C_{k_1}^{(m)} C_{k_2}^{(m)} \dots C_{k_{m+1}}^{(m)}, \quad \text{for } n, m \in \mathbb{N}.$$

In closed form, the n^{th} Fuss-Catalan number is given by

$$C_n^{(m)} = \frac{1}{mn+1} \binom{(m+1)n}{n}.$$

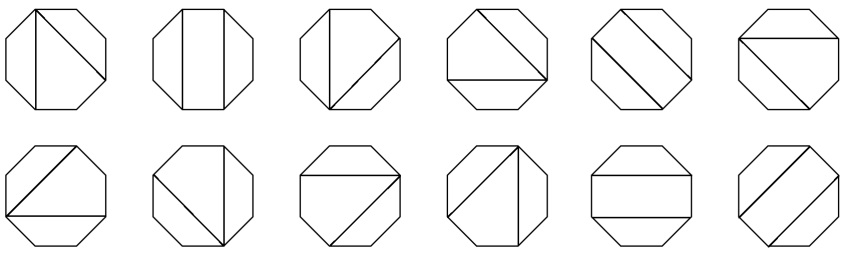

Figure 1.9: The $C_3^{(2)} = 12$ quadrangulations of an octagon.

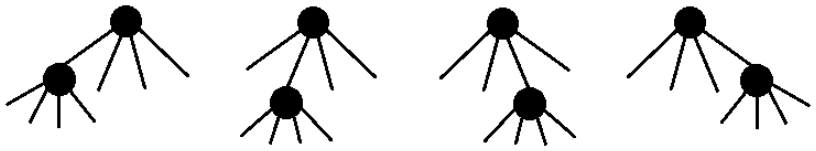

Figure 1.10: The $C_2^{(3)} = 4$ 4-ary trees with 2 parent nodes.

1.4 The m-Tamari lattices

Diagonal coinvariants in $m+1$ sets of variables generalize the coinvariant algebra obtained from the symmetric group action on polynomials. (See [8] for important results on the $m = 1$ case.) In his study of diagonal coinvariants for $m \geq 1$, Francois Bergeron [2] generalized the Tamari lattices T_n to the m-Tamari lattices $T_n^{(m)}$, posets with $C_n^{(m)}$ many elements. Naturally, researchers have been interested in understanding how properties of the Tamari lattices extend, or do not extend, to the m-Tamari case.

To illustrate this, we will consider the m-Tamari lattices on $(m+2)$-angulations of an $(mn+2)$-gon. We will arrive at this realization of the lattices by first considering the m-Tamari lattices on m-Dyck paths, and making use of a bijection from m-Dyck paths to $(m+2)$-angulations.

An m-Dyck path is a sequence of unit length North and East steps in $\mathbb{R}^2$ from $(0,0)$ to (mn,n) that does not go below the line $y = \frac{1}{m}x$. In this context, the rule for moving up in the m-Tamari lattices is as follows: if possible, find an East step followed by a North step in some m-Dyck path. Draw a line with slope $\frac{1}{m}$ from the bottom of the North step to wherever it reconnects with the path. Since the path begins and ends on the line

$y = \frac{1}{m}x$ and never goes below, we are guaranteed that a parallel line from the bottom of a North step will intersect the path at some point. Remove the East step of interest and insert it immediately to the right of where the diagonal line reconnected with the path. See Figure 1.11 for an example of this cover relation for $m = 2$, $n = 3$. Notice that since we can find two East steps which are followed by North steps for the lower 2-Dyck path, the latter has two upper covers.

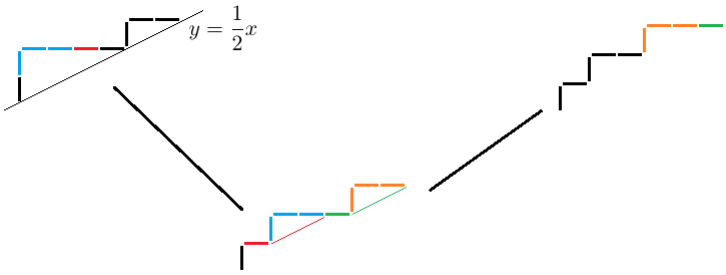

Figure 1.11: The covers for a 2-Dyck path in $T_3^{(2)}$.

A bijection from m-Dyck paths to $(m+2)$-angulations is described by Drew Armstrong, Brendon Rhoades, and Nathan Williams [1] as follows: start by adding an East step onto the end of the m-Dyck path, so that it now ends at the point $(mn+1, n)$ in $\mathbb{R}^2$. Do a similar trick as before and draw a line with slope $\frac{n}{mn+1}$ from the bottom of each North step to wherever it reconnects with the path, which will no longer be at a point on the integer lattice since n and $mn+1$ are coprime. If the line begins at a point with x-coordinate c and ends at a point with x-coordinate d, then draw the diagonal from vertex $c+1$ to vertex $\lceil d \rceil + 1$ in the angulation. See Figure 1.13 for an

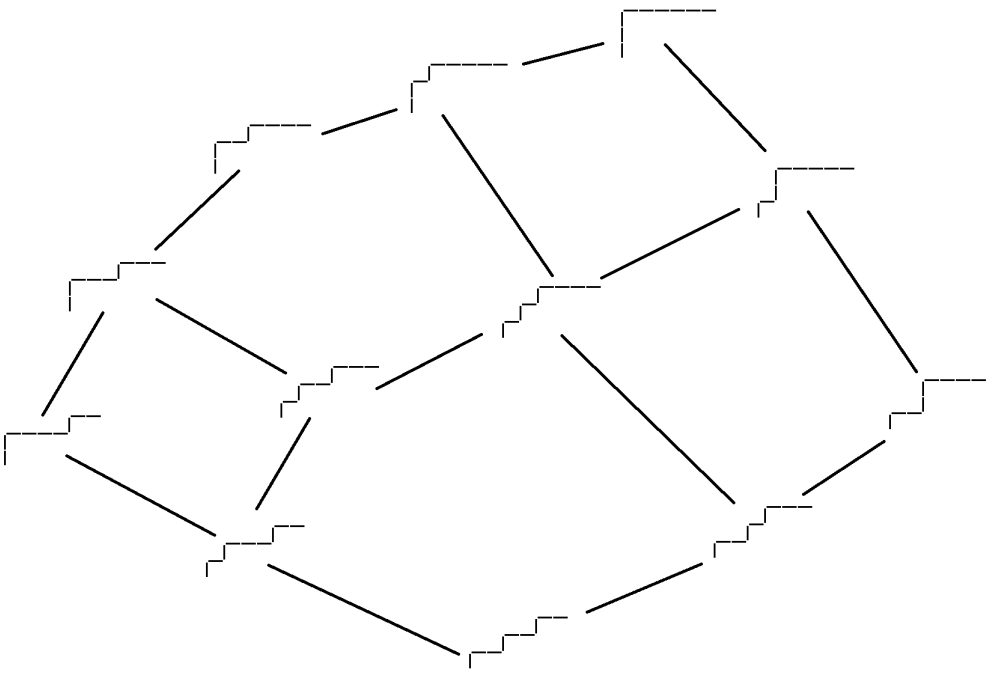

Figure 1.12: $T_3^{(2)}$ has $C_3^{(2)} = 12$ elements.

example of the bijection, and Figure 1.14 for $T_3^{(2)}$ obtained by applying this bijection to the lattice in Figure 1.12:

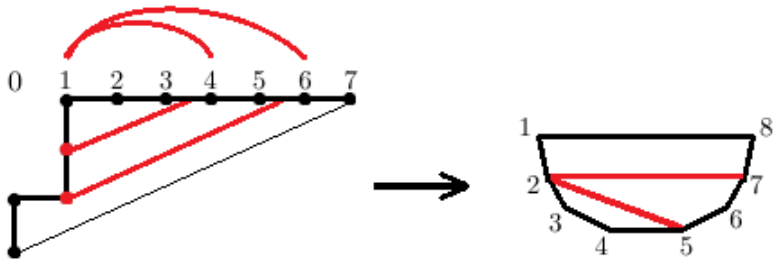

Figure 1.13: A bijection from m-Dyck paths to $(m+2)$-angulations.

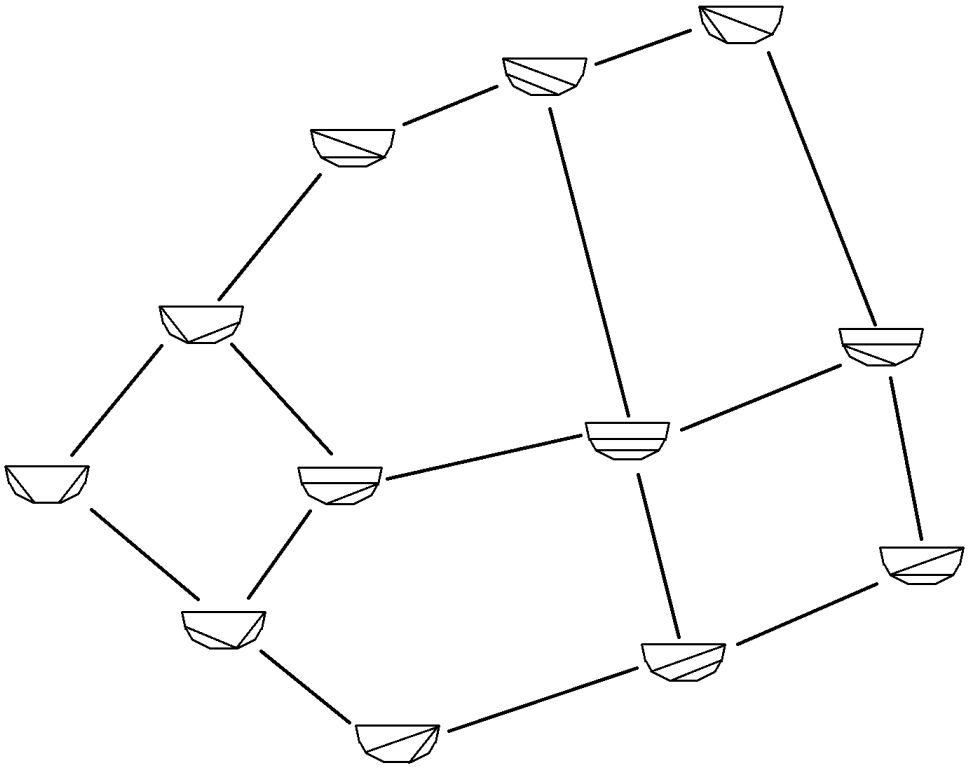

Figure 1.14: $T_3^{(2)}$ realized on quadrangulations of an octagon.

Notice that $T_3^{(2)}$ on angulations does not obey the nice description regarding slopes of the diagonals that is present for the $m = 1$ case. See Bergeron's paper [3] for some nice pictures of how these lattices behave when m and n vary.

1.5 Coxeter groups

1.5.1 General Coxeter groups

To better understand the background which led Stump et al. to the family of m-Cambrian lattices of interest in this thesis, we should first define a very special class of groups in both combinatorics and geometry.

Definition 1.5.1. *A **Coxeter group** W is an abstract group with a presentation of the form $W = \langle s_1, s_2, \ldots, s_n \mid (s_i s_j)^{m_{ij}} = e \rangle$, where the s_i are the generators for W, e is the identity in W, and $m_{ij} \in \mathbb{Z} \cup \{\infty\}$ has the following properties:*

- $m_{ii} = 1$ *(that is, $s_i = {s_i}^{-1}$ for all generators of W),*
- $m_{ij} \geq 2$ *for $i \neq j$, and*
- $m_{ij} = \infty$ *indicates the absence of a relation concerning $s_i s_j$.*

Since the s_i generate the group, every element in the group can be expressed as a product of these generators. We refer to specific expressions for elements of W as *words*. There are many words which all determine the same element of W. If for an element $w = s_{i_1} s_{i_2} \ldots s_{i_k}$, k is minimal with respect to all other ways to express w, then we say that k is the *length* of w and that $s_{i_1} s_{i_2} \ldots s_{i_k}$ is a *reduced expression* for w. If W is finite, there exists a unique longest element $w_0 \in W$ such that the length of w_0 is greater than the length of any other $w \in W$. A *Coxeter element* $c \in W$ is a product of

all generators of W in some fixed order. We refer to [9] for an explaination of these matters.

It turns out that every finite Coxeter group can be realized as a group of Euclidean isometries generated by reflections s_i. It is for this reason that we call the s_i *simple reflections*.

For example, the Coxeter group

$$B_n = \langle s_1, s_2, \ldots, s_n \mid (s_1 s_2)^4 = (s_i s_{i+1})^3 = (s_i s_j)^2 = {s_k}^2 = e \text{ for } i \geq 2,\ |i-j| \geq 2 \rangle$$

is isomorphic to the symmetry group of a regular n-dimensional cube. See Figure 1.15 for an example where $n = 3$.

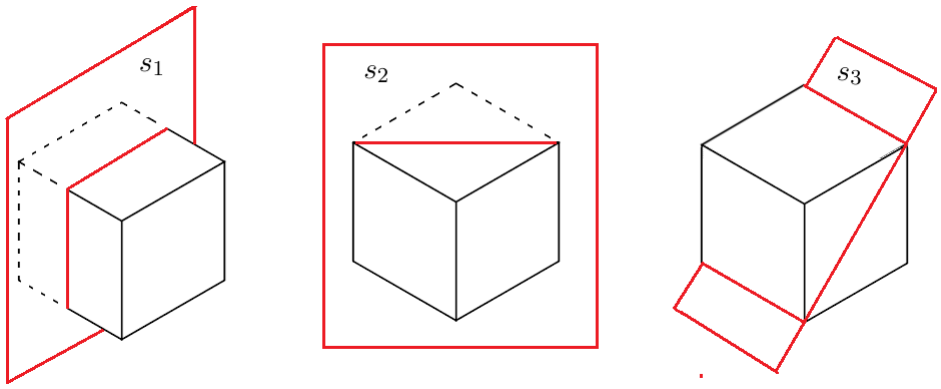

Figure 1.15: Three planes of reflection of the cube generate its entire symmetry group.

The relations for B_3 are

$$(s_1 s_2)^4 = (s_2 s_3)^3 = (s_1 s_3)^2 = {s_k}^2 = e.$$

The relation $(s_1 s_3)^2 = e$ can be rewritten as $s_1 s_3 = s_3 s_1$, which shows that first applying the reflection s_1 followed by s_3 sends points on the cube to the same positions they are sent to when we apply the reflections in opposite order. This manifests itself in Figure 1.15 as the mirrors of reflection for s_1 and s_3 being perpendicular to each other.

The longest element in B_3 is $w_0 = s_1 s_2 s_3 s_1 s_2 s_3 s_1 s_2 s_3$. Note that there can be several reduced expressions for any element $w \in W$. The possible Coxeter elements in this group are $s_1 s_2 s_3$, $s_1 s_3 s_2$, $s_2 s_3 s_1$, and $s_3 s_2 s_1$.

1.5.2 The Coxeter group A_{n-1}

The family of m-Cambrian lattices that is of interest in this thesis arise from the Coxeter group

$$A_{n-1} = \langle s_1, s_2, \ldots, s_{n-1} \mid (s_i s_{i+1})^3 = (s_i s_j)^2 = {s_k}^2 = e \text{ for } |i-j| \geq 2 \rangle.$$

This group is isomorphic to the symmetry group of a regular $(n-1)$-dimensional simplex. See Figure 1.16 for an example where $n = 3$.

The longest element of A_2 is $w_0 = s_1 s_2 s_1 = s_2 s_1 s_2$ and the two possible Coxeter elements are $s_1 s_2$ and $s_2 s_1$.

In general, all Coxeter elements of A_{n-1} are conjugate, and each has order n. The longest element w_0 is unique and it has order 2. Also, the length of the longest element in A_{n-1} is $\binom{n}{2}$.

Furthermore, A_{n-1} is isomorphic to the symmetric group S_n. We

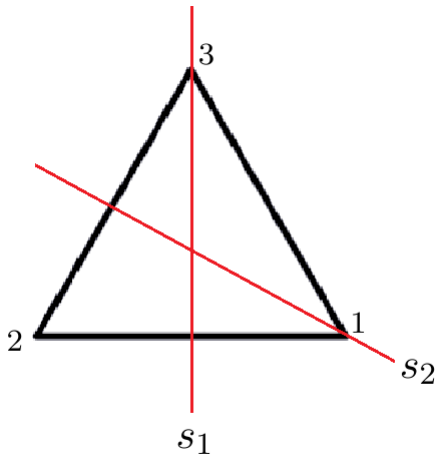

Figure 1.16: Just two lines of reflection of the equilateral triangle generate its entire symmetry group.

can define this isomorphism by the map $\sigma : A_{n-1} \to S_n$ where $\sigma(s_i) = (i, i+1)$, a transposition. Thus, S_3 is isomorphic to the symmetry group of the equilateral triangle as well, and we interpret the transposition $(i, i+1)$ as the reflection that interchanges vertices i and $i+1$.

In this representation, the Coxeter element

$$c = s_1 s_2 \dots s_{n-1} = (1, n, , n-1, \dots, 3, 2)$$

is an n-cycle. Note that here, we are composing permutations from left to right.

Chapter 2

Some Fuss-Catalan objects

In this chapter, we will introduce a few Fuss-Catalan objects and describe how they are related to one another.

2.1 Facets of m-cluster complexes

Consider the generators $s_1, s_2, \ldots, s_{n-1}$ of the group A_{n-1}. Arrange these generators in staggered rows with s_i in the i^{th} row for $1 \leq i \leq n-1$ (see Figure 2.1 for an example with A_4).

$$
\begin{array}{ccccccccccccccccc}
\cdots & & s_4 & & s_4 & & s_4 & & s_4 & & s_4 & & s_4 & & s_4 & & \ldots \\
\cdots & s_3 & & s_3 & & s_3 & & s_3 & & s_3 & & s_3 & & s_3 & & s_3 & \cdots \\
\cdots & & s_2 & & s_2 & & s_2 & & s_2 & & s_2 & & s_2 & & s_2 & & \ldots \\
\cdots & s_1 & & s_1 & & s_1 & & s_1 & & s_1 & & s_1 & & s_1 & & s_1 & \ldots
\end{array}
$$

Figure 2.1: Arrange the generators of A_{n-1} in staggered rows.

In this diagram, a given Coxeter element from A_{n-1} manifests itself in a path from the top row to the bottom. To construct a path from a Coxeter element $c = s_{i_1} s_{i_2} \dots s_{i_{n-1}}$, where $i_1, i_2, \dots i_{n-1}$ is a permutation of $1, 2, \dots, n-1$, we start at the top of the diagram at s_{n-1}. We then proceed down the diagram moving left if s_{j-1} appears to the left of s_j in c, and moving right if s_{j-1} appears to the right of s_j in c, for $j \in \{2, 3, \dots, n-1\}$. We reproduce a factorization for this Coxeter element by scanning the $s'_j s$ in the path in left to right order. In Figure 2.2 we look at two possible Coxeter elements, $c = s_1 s_2 s_3$ and $c = s_1 s_3 s_2 = s_3 s_1 s_2$. A reduced expression for the longest element w_0 in A_{n-1} can be read from the diagram by multiplying $\binom{n}{2}$ of the generators to the right of the Coxeter element [12, Lemma 2.18]. For example, in Figure 2.2, the Coxeter element $c = s_1 s_2 s_3$ results in a reduced expression $w_0 = s_1 s_2 s_3 s_1 s_2 s_1$ and the Coxeter element $c = s_1 s_3 s_2$ results in a reduced expression $w_0 = s_1 s_3 s_2 s_1 s_3 s_2$.

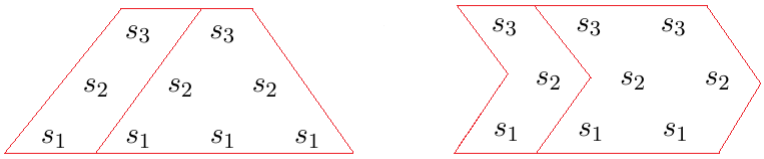

Figure 2.2: Coxeter element $c = s_1 s_2 s_3$ on the left and $c = s_1 s_3 s_2 = s_3 s_1 s_2$ on the right.

Another copy of w_0 can be read from $\binom{n}{2}$ of the generators to the right of the first copy of w_0. This can easily be seen in Figure 2.3 for the case where the Coxeter element is $c = s_1 s_3 s_2$. However, for the case where

the Coxeter element is $c = s_1 s_2 s_3$, we need to use some of the relations from A_3 to see this. That is,

$$\begin{aligned}
w_0 &= s_1 s_2 s_3 s_1 s_2 s_1 \\
&= s_1 s_2 s_1 s_3 s_2 s_1 && (s_1 s_3 = s_3 s_1) \\
&= s_2 s_1 s_2 s_3 s_2 s_1 && (s_1 s_2 s_1 = s_2 s_1 s_2) \\
&= s_2 s_1 s_3 s_2 s_3 s_1 && (s_2 s_3 s_2 = s_3 s_2 s_3) \\
&= s_2 s_1 s_3 s_2 s_1 s_3 && (s_1 s_3 = s_3 s_1) \\
&= s_2 s_3 s_1 s_2 s_1 s_3 && (s_1 s_3 = s_3 s_1) \\
&= s_2 s_3 s_2 s_1 s_2 s_3 && (s_1 s_2 s_1 = s_2 s_1 s_2) \\
&= s_3 s_2 s_3 s_1 s_2 s_3. && (s_2 s_3 s_2 = s_3 s_2 s_3)
\end{aligned}$$

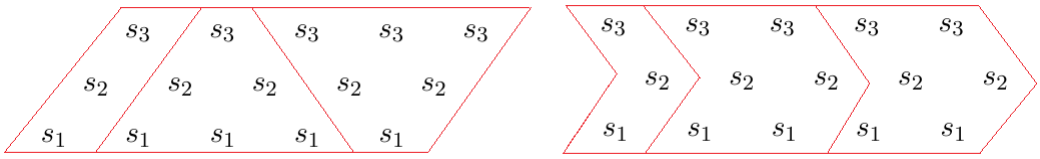

Figure 2.3: Coxeter element $c = s_1 s_2 s_3$ on the left and $c = s_1 s_3 s_2 = s_3 s_1 s_2$ on the right.

Note that in this calculation, we do not actually use the fact that ${s_k}^2 = e$.

The relations for A_{n-1} are

$$(s_i s_{i+1})^3 = (s_i s_j)^2 = {s_k}^2 = e \text{ for } |i - j| \geq 2.$$

We can rewrite these in the following way:

$$(s_i s_{i+1})^3 = e \implies s_i s_{i+1} s_i = s_{i+1} s_i s_{i+1}$$

and

$$(s_i s_j)^2 = e \implies s_i s_j = s_j s_i \text{ for } |i-j| \geq 2.$$

We drop the relations ${s_k}^2 = e$ and use only the rewritten relations above to abstractly define the *braid group*

$$\text{Braid}_{n-1} = \langle s_1, s_2, \ldots, s_{n-1} \mid s_i s_{i+1} s_i = s_{i+1} s_i s_{i+1},\ s_i s_j = s_j s_i \text{ for } |i-j| \geq 2 \rangle.$$

Here, we are abusing notation by letting s_k refer as well to the generators of Braid_{n-1}. Note that the finite group A_{n-1} is a quotient of Braid_{n-1}.

In the Coxeter group, we have that ${w_0}^2 = e$ [5, Proposition 2.3.2]. In the braid group, ${w_0}^2$ is the element which is obtained by concatenating two reduced expressions for the longest element in the corresponding Coxeter group. In general, ${w_0}^m$ is the element obtained by concatenating m reduced expressions for the longest element in the corresponding Coxeter group.

For the remainder of this thesis, we are going to concern ourselves with Coxeter elements of the form $c = s_1 s_2 \ldots s_{n-1}$, so that the diagrams of interest look like the type in the left of Figures 2.2 and 2.3. That is, the diagram has a strip of the $n-1$ generators on the left, followed by m copies

of w_0 arranged in triangles. We call these diagrams *linear type* A_{n-1}. Linear refers to the order in which we multiply the generators of the Coxeter element, and A_{n-1} refers to the fact that the braid group Braid_{n-1} corresponds to the Coxeter group A_{n-1}.

The Fuss-Catalan objects obtained from these diagrams are *facets of m-cluster complexes* [12]. By definition, a facet of the m-cluster complex is a set of $n-1$ of the generators in the diagram such that removing these generators gives us a reduced expression for ${w_0}^m$ in Braid_{n-1} when we read the remaining generators in the diagram from left to right. An example can be seen of the 12 such facets of the m-cluster complex (or facets) in Figure 2.4 where $n = 3$ and $m = 2$. In this case, the longest element in A_2 is $w_0 = s_1 s_2 s_1 = s_2 s_1 s_2$. Recall that in the braid group, we no longer have the property that ${s_k}^2 = e$, so $s_1 s_2 s_2 s_1 s_2 s_2$ is a legitimate reduced expression for ${w_0}^2$.

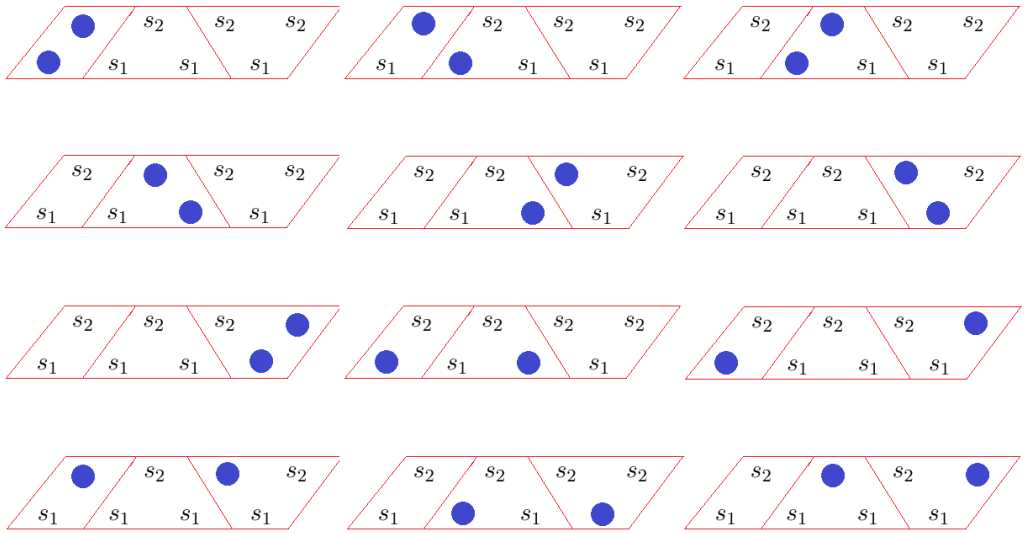

Figure 2.4: The $C_3^{(2)} = 12$ facets obtained by reading reduced expressions for ${w_0}^2$ from left to right.

2.2 $(m+2)$-angulations of an $(mn+2)$-gon

As mentioned in the previous chapter, $C_n^{(m)}$ counts the number of $(m+2)$-angulations of an $(mn+2)$-gon. I will show that there are the same number of generators in the diagrams above as there are possible diagonals in an $(m+2)$-angulation of an $(mn+2)$-gon.

Since the diagrams above consist of a strip of $n-1$ generators on the left followed by m copies of w_0 (whose length is $\binom{n}{2}$ for A_{n-1}), there are

$$(n-1) + m\binom{n}{2} = \frac{1}{2}(n-1)(mn+2)$$

generators in each diagram.

To find how many possible diagonals there are in an $(m+2)$-

angulation of an $(mn+2)$-gon, first consider the angulation where each diagonal contains the vertex 1 (we call this the *fan* at vertex 1). From Figure 2.5, we can observe that there are exactly $n-1$ diagonals containing 1 as a vertex. So there are $n-1$ diagonals containing any given vertex x, and there are $mn+2$ vertices to choose from. However, we need to be wary of double counting since the diagonals (x,y) and (y,x) are the same. Hence, there are $\frac{1}{2}(n-1)(mn+2)$ possible diagonals in an $(m+2)$-angulation of an $(mn+2)$-gon.

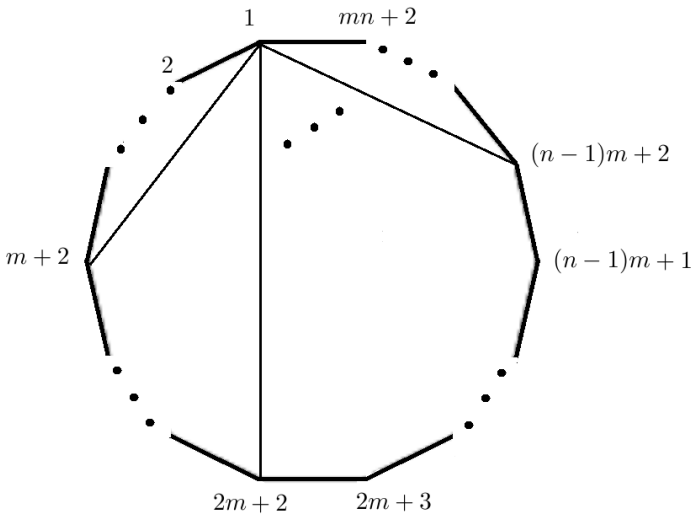

Figure 2.5: There are $n-1$ diagonals containing the vertex 1.

Since the number of generators in each diagram and the number of possible diagonals in an $(m+2)$-angulation of an $(mn+2)$-gon is the same, we can arrange the diagonals in a similar fashion. That is, we can arrange $n-1$ of the diagonals in a strip on the left followed by m triangles of $\binom{n}{2}$

diagonals each.

Begin by filling the $n-1$ positions in the leftmost strip with diagonals containing 1 as a vertex so that row i of the strip contains the diagonal $(1, im+2)$ for $1 \leq i \leq n-1$. Suppose we know the position of some diagonal (x, y) in a diagram. If we perform the glide reflection described by moving n columns to the right followed by reflection in the horizontal bisector of the diagram, we label the new position with the diagonal $(x-1, y-1)$ mod $(mn+2)$. That is, a rightward glide reflection in the diagram corresponds to a clockwise rotation of the diagonal by one step. Refer to 2.6 for an example where $n = 4$ and $m = 3$. Imagine we use a pair of scissors to cut around the border of the diagram and then glue the right edge of the border to the left edge. For even values of m this will give us a loop, and for odd values of m we get a Möbius strip. This helps to resolve the issue of running off the right end of the diagram when using the above labelling rule; when you exit right from row i, then re-enter from the left in row $n-i$ if m is odd, or re-enter from the left in row i if m is even.

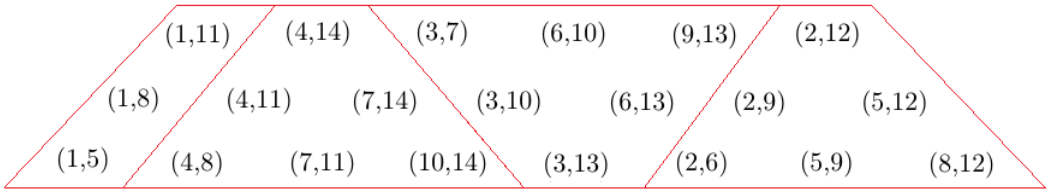

Figure 2.6: Arranging the diagonals for a 5-angulation of a 14-gon.

Since the leftmost strip contains all of the diagonals with 1 as a

vertex, it can be indexed by the number 1. When we take a rightward glide reflection of the entire strip, we will obtain a strip indexed by the number $mn+2$. By taking a rightward glide reflection of this second strip, we obtain a third strip indexed by the number $mn+1$. Continuing this process allows us to see that each strip in the diagram is indexed by exactly one of the numbers in the set $\{1, 2, \ldots, mn+2\}$.

Interestingly, this allows us to realize the $mn+2$ edges of the $(mn+2)$-gon as lying just outside of the border to the dot diagram. This is illustrated in Figure 2.7.

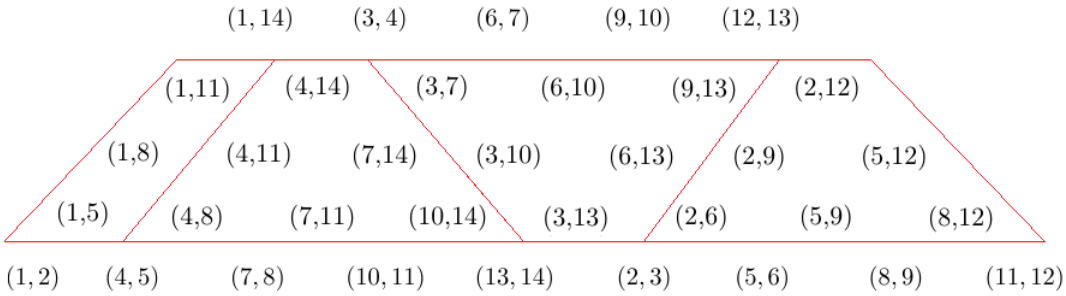

Figure 2.7: The edges of the $(mn+2)$-gon are realized above and below the dot diagram.

If we label the vertices of an octagon in the usual way, then the 8 distinct diagonals are $(1,4)$, $(1,6)$, $(2,5)$, $(2,7)$, $(3,6)$, $(3,8)$, $(4,7)$, and $(5,8)$. Refer to Figure 2.8 for the $C_3^{(2)} = 12$ diagrams, each corresponding to a quadrangulation of an octagon. We have circled the diagonals present in each angulation.

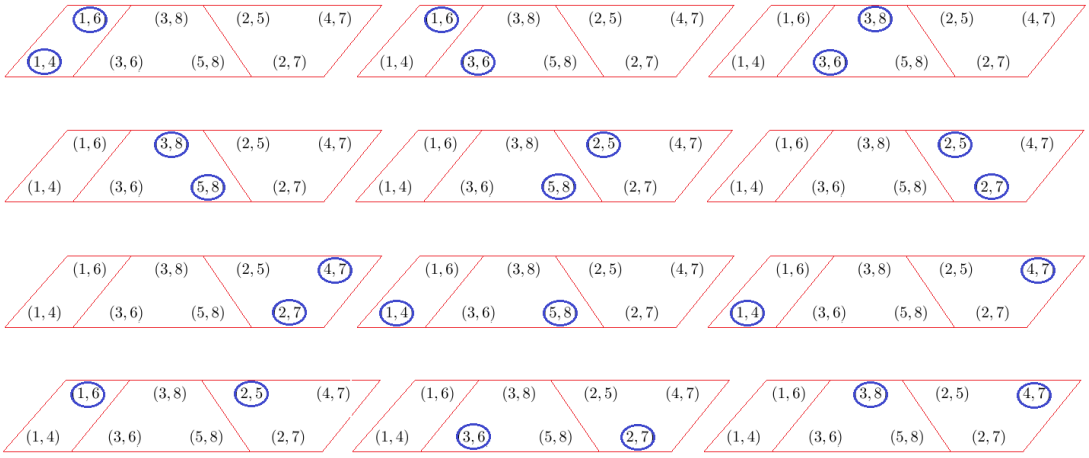

Figure 2.8: The $C_3^{(2)} = 12$ quadrangulation of an octagon.

2.3 Dot diagrams

Imagine instead of having diagonals or Coxeter generators in each position in the diagram, we have empty dots. If we are starting from a diagram with Coxeter generators, we shade the $n-1$ dots corresponding to the generators in each facet (shaded blue in Figure 2.4). If we are starting from a diagram with diagonals, we shade the $n-1$ dots corresponding to the diagonals in the angulation (circled in Figure 2.8).

An important result [12, Theorem 5.20] states that the set of $C_n^{(m)}$ dot diagrams produced is the same, regardless of which type of diagram we begin with. Refer to Figure 2.9 to see that Figures 2.4 and 2.8 will produce the same $C_3^{(2)} = 12$ dot diagrams.

However, this result was proved for diagrams obtained from a different choice of Coxeter element and a different diagonal labelling procedure.

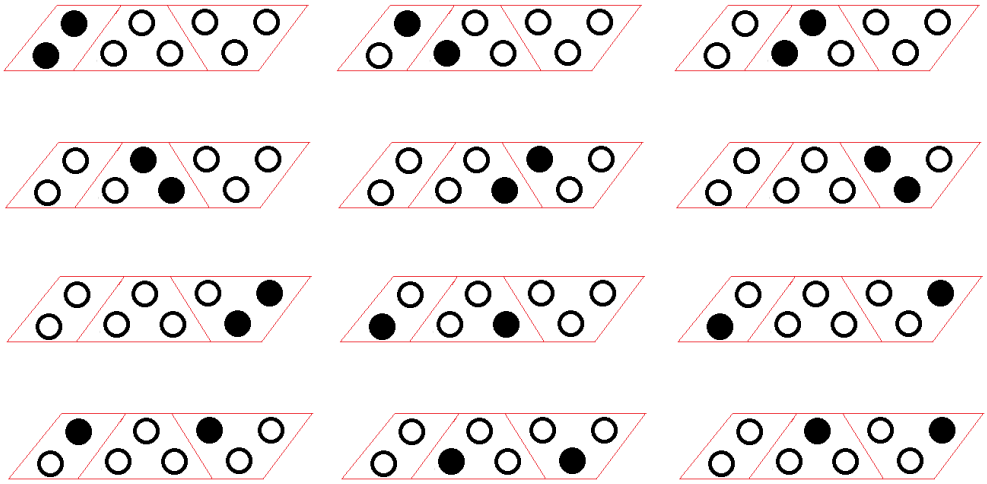

Figure 2.9: The same $C_3^{(2)} = 12$ dot diagrams are obtained whether we begin with Figure 2.4 or 2.8.

We will give an argument for why the result is still true for our choice of Coxeter element and diagonal labelling procedure.

First, let us consider an angulation A whose diagonal (a, b) flips to the diagonal (c, d) in angulation B. From observing Figure 2.10, we can see that the diagonals (a, d) and (c, b) must be present in both A and B. In the dot diagram, this translates to Figure 2.11.

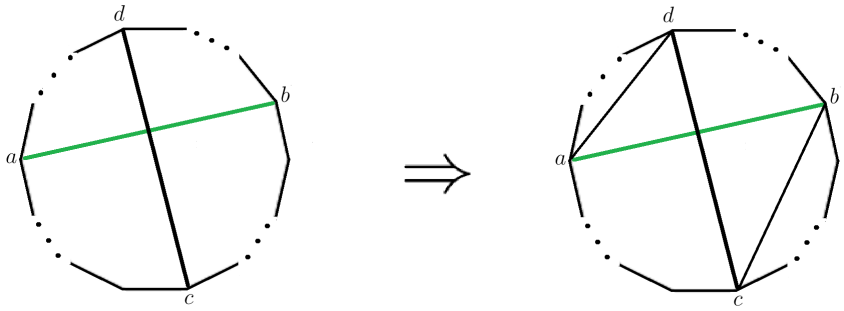

Figure 2.10: If (a, b) flips to (c, d), then (a, d) and (c, b) are both present.

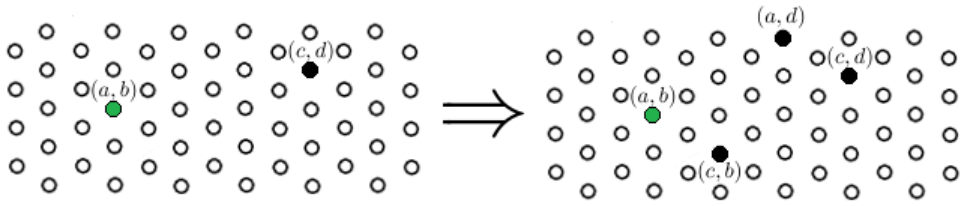

Figure 2.11: If (a, b) flips to (c, d), then (a, d) and (c, b) are both present.

In joint work, Sergey Fomin and Nathan Reading [7] establish a correspondence between diagonals of angulations and dots in a slightly different dot diagram. They obtain their dot diagrams by choosing a different Coxeter element than we are considering. It is possible to give an explicit argument that the rule we use for labelling dots as diagonals agrees with the way that Fomin and Reading label their dots. However this argument would be tedious, and not so enlightening. We will instead present an argument suggested by Professor Thomas. Although this argument uses some concepts to which we do not otherwise refer in this thesis, it will hopefully feel more intuitive to the reader.

Although Fomin and Reading make a different choice of Coxeter element than we do, [12, Proposition 5.17] says that there is a procedure for passing from a dot diagram using Coxeter element c to a dot diagram using a different Coxeter element c'. That is, if we have two Coxeter elements $c = s_{i_1} s_{i_2} ... s_{i_{n-1}}$ and $c' = s_{i_2} ... s_{i_{n-1}} s_{i_1}$, the corresponding dot diagrams differ by moving a single dot from the lefthand end to the righthand end, without changing its vertex labelling.

So if we label our dots using Fomin and Reading's procedure, and

then pass from their dot diagram to ours, we will have some association of dots in our dot diagram and diagonals. We want to show that the dots will have the same labelling if we use our labelling procedure.

As mentioned above, if there are two dots (a, b) and (c, d) which are related by a rightward flip, then there are two diagonals which are forced to appear, namely (a, d) and (c, b). From the m-cluster category perspective [15], it is clear that the forced dots that appear are the ones that create a parallelogram with (a, b) and (c, d) (if we use the Fomin-Reading labelling). This is also true of our labelling. From this, we can establish that all of the dots in a given diagonal line in the Fomin-Reading labelling, share a vertex. Note that this is also true of our labelling.

Now it is just a matter of checking that the order in which the diagonals appear is the same in the Fomin-Reading labelling and in our labelling. This follows from the fact that the Fomin-Reading labelling and our labelling both satisfy that a rightwards glide reflection rotates the diagonal clockwise by one step.

For the remainder of this thesis, we will use the following definition for dot diagrams.

Definition 2.3.1. *A **dot diagram** consists of a strip of $n-1$ dots on the left of the diagram followed to the right by m triangles containing $\binom{n}{2}$ dots each. The shaded dots correspond to the diagonals present in the corresponding $(m+2)$-angulation of an $(mn+2)$-gon (when the dots are labelled according to the procedure described above).*

This is a more accessible definition for our purposes as it allows us to step away from Coxeter groups and facets of m-cluster complexes, the context in which these diagrams were originally developed. Now we can use the more accessible $(m+2)$-angulations of an $(mn+2)$-gon to help us study the properties of dot diagrams.

Chapter 3

A partial order on $(m+2)$-angulations

Now that we have familiarized ourselves with dot diagrams and how they are related to facets of m-cluster complexes and $(m+2)$-angulations of an $(mn+2)$-gon, we can begin to discuss a partial order on the set of dot diagrams. The Hasse diagram of the resulting poset with $C_n^{(m)}$ many elements is an m-Cambrian lattice of the type we are interested in, which we denote $\mathrm{Cam}_n^{(m)}$. We will look at two different descriptions for a partial ordering, and will then prove that the two descriptions are equivalent.

3.1 The first partial order: rotation order

We say that a configuration of shaded dots in a dot diagram is *legal* if it corresponds to an $(m+2)$-angulation of an $(mn+2)$-gon. Given the positions of $n-2$ of the $n-1$ shaded dots, we say that the remaining shaded dot is in a *legal position* if the resulting configuration of shaded dots is legal. Then we can describe the partial order on legal configurations of shaded dots as the transitive closure of the relation defined by moving a single shaded dot to the next legal position to the right. We call this partial ordering the *rotation order*, denoted "$\leq_r$". This order is equivalent to the order defined in [12, Definition 5.39]. See Figure 3.1 for $\mathrm{Cam}_3^{(2)}$ containing the $C_3^{(2)} = 12$ dot diagrams from Figure 2.9.

In Figure 3.2, we draw the corresponding angulations in place of the dot diagrams from Figure 3.1. We see that moving a dot to the right to its next legal postion in the dot diagram translates to rotating a diagonal clockwise by one step in the corresponding angulation. Although we haven't proved this yet, we will see later that this property is true in general.

In Chapter 0, it was mentioned that for the $m = 1$ case we recover the Tamari lattices. That is, $\mathrm{Cam}_n^{(1)} = T_n$. This can be seen by comparing Figures 1.8 and 3.4, with the dot labelling given in Figure 3.3. Note that in this case, clockwise rotation of a diagonal by one step reduces to flipping a diagonal in some quadrilateral to a diagonal with higher vertex labelling. This is exactly how the cover relations are defined for the Tamari lattices.

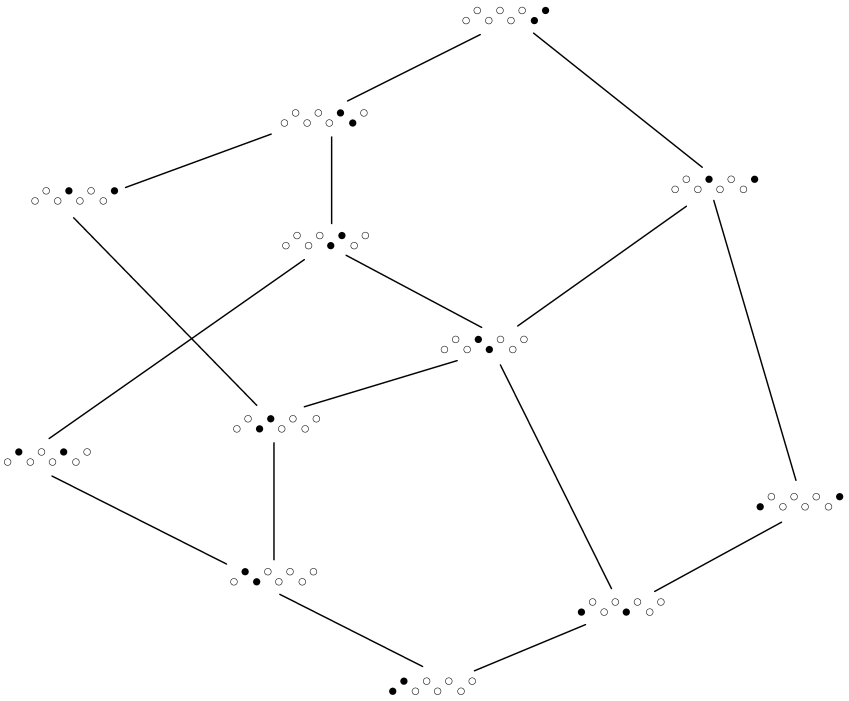

Figure 3.1: $\mathrm{Cam}_3^{(2)}$ realized on dot diagrams. The cover relation is moving a shaded dot to the right to its next legal position.

We can describe the cover relations quite nicely just from looking at the angulations. But in order to do this, we need to rethink the way we label the vertices of the $(mn+2)$-gon. It turns out that this labelling might be a more natural way to label the polygon, and will lead to a dot labelling which is easier to describe as well.

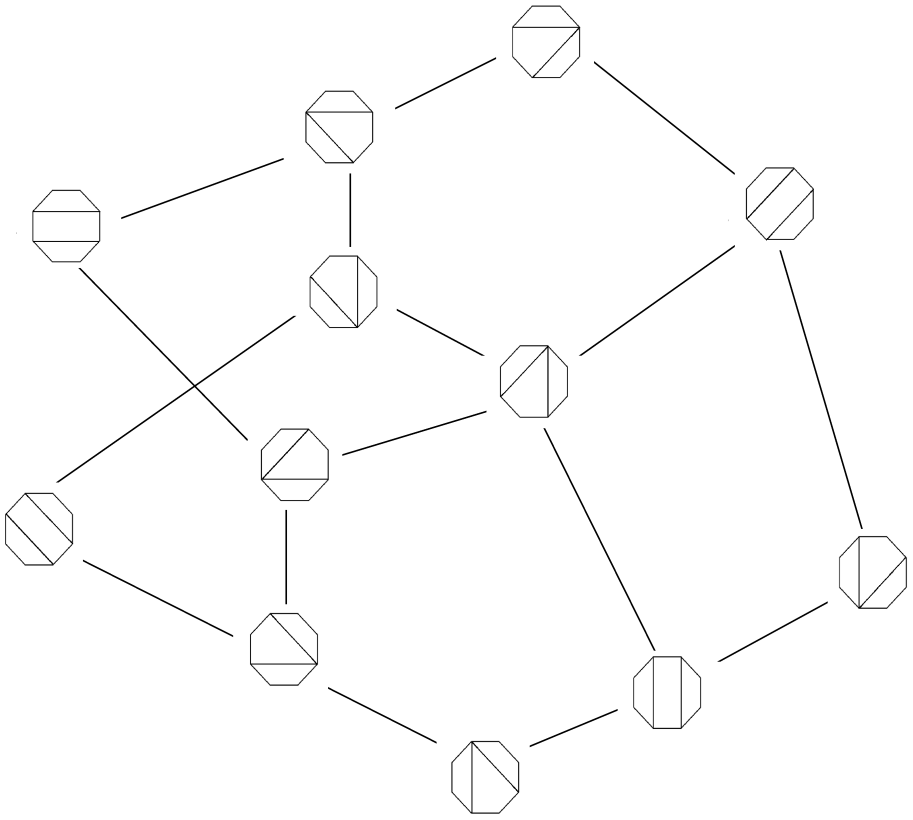

Figure 3.2: $\mathrm{Cam}_3^{(2)}$ realized on quadrangulations of an octagon. Note that this lattice is distinct from $T_3^{(2)}$ seen in Figure 1.14.

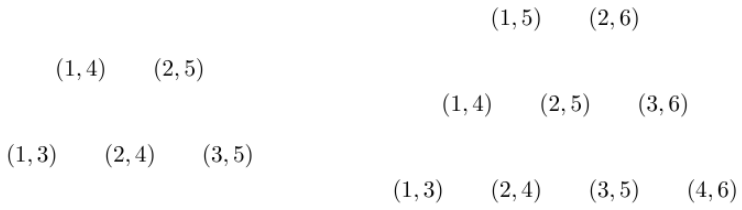

Figure 3.3: The labelling of dots for $n = 3$ (left) and $n = 4$ (right). Note that $m = 1$ in both cases.

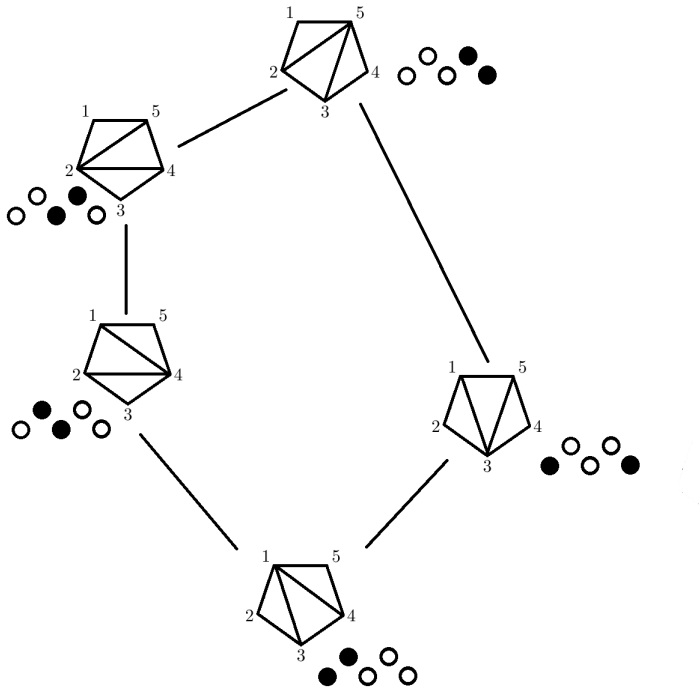

Figure 3.4: $\mathrm{Cam}_3^{(1)} = T_3$.

3.2 Alternative vertex labelling

Roughly speaking, the procedure we use to label the vertices of an $(mn+2)$-gon is as follows. We first choose a vertex and label it with the number 1. Then move m steps counter clockwise and call this vertex 2. Continue this procedure until all vertices are labelled, i.e., for $mn+2$ steps. Note that for $m = 1$, we recover the conventional vertex labelling. However, this procedure does not quite work for even m, as we shall discuss below.

In general, when we move around an n-sided polygon with step size

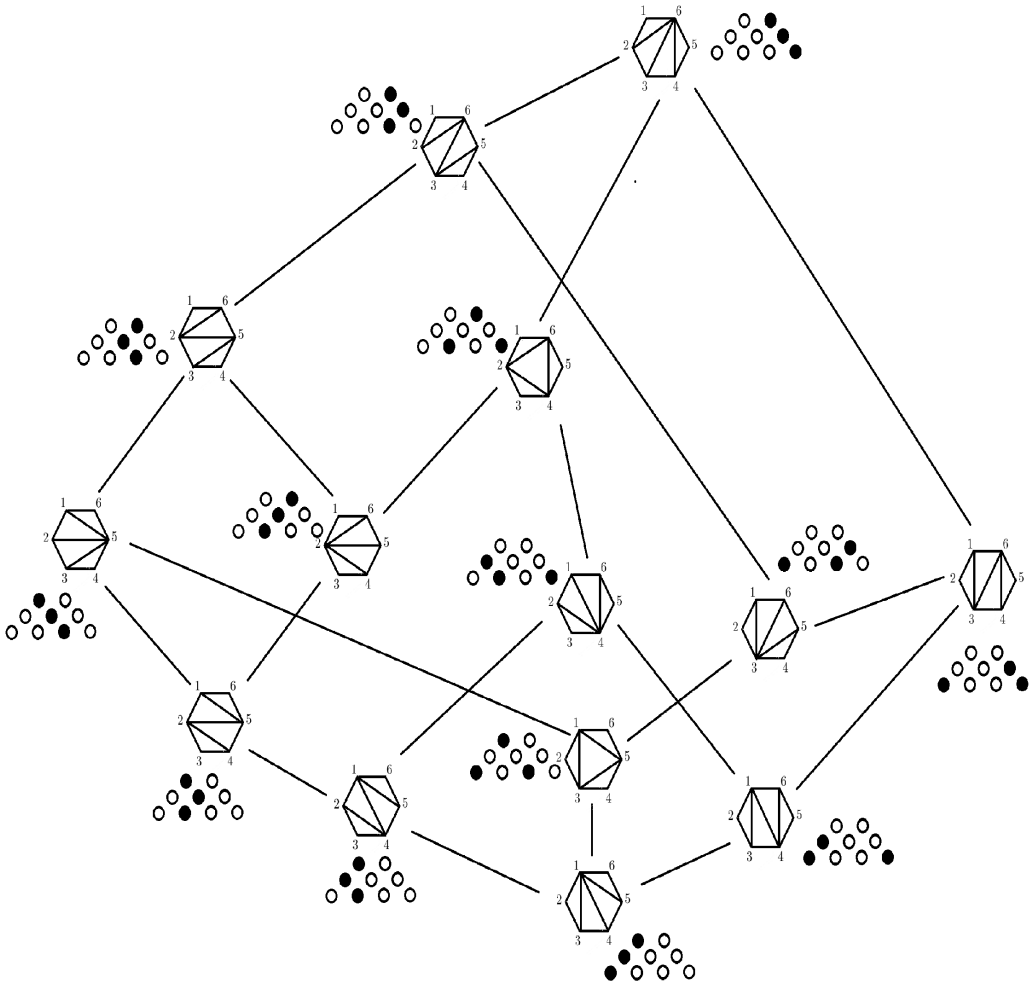

Figure 3.5: $\mathrm{Cam}_4^{(1)} = T_4$.

d, the number of revolutions made around the center of the n-gon until we reach the vertex we started with is $\frac{d}{\gcd(n,d)}$. We call this the winding number. The number of vertices covered in the $\frac{d}{\gcd(n,d)}$ revolutions around the center of the polygon is $\frac{n}{\gcd(n,d)}$.

So in our case, when we trek around our $(mn+2)$-gon with step

size m, the winding number is $\frac{m}{\gcd(mn+2,m)}$ and the number of vertices covered before we reach the vertex we started with is $\frac{mn+2}{\gcd(mn+2,m)}$.

Suppose that $\gcd(mn+2, m) = q$, so that $m = pq$ and $mn+2 = rq$ for integers p and r. Then $pqn + 2 = rq$ so that $\frac{2}{q} = r - pn \in \mathbb{Z}$, and hence $q = 1$ or $q = 2$. Let us look at two cases seperately.

Case I: m is odd.

If m is odd, then 2 is not one of its divisors. By the above argument that $q = \gcd(mn+2, m)$ only takes on values 1 or 2, it must be the case that $\gcd(mn+2, m) = 1$. Thus the winding number is m, and all $mn+2$ vertices are covered before we reach the vertex we started with.

Refer to Figure 3.6 for the example where $n = 4$ and $m = 3$.

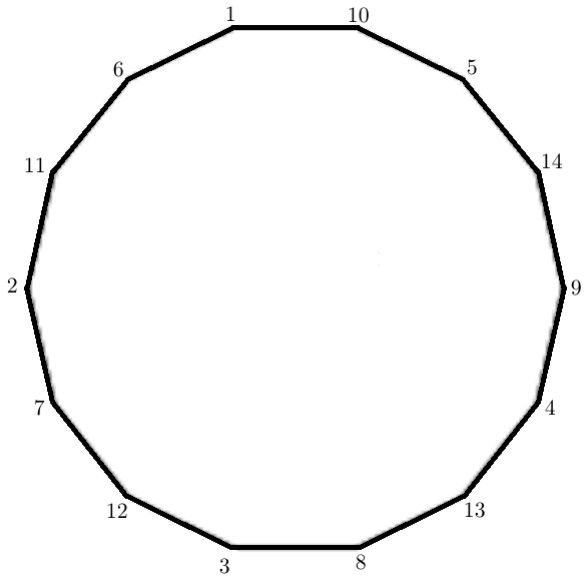

Figure 3.6: Labelling vertices of the 14-gon using the rule described above.

We can see from the corresponding dot diagram in Figure 3.7 that

the vertex labelling is strictly increasing as we move from left to right.

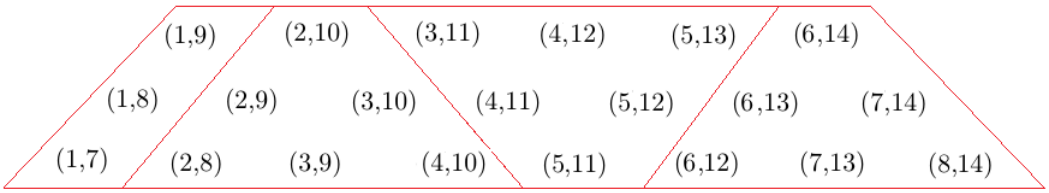

Figure 3.7: The dot diagram corresponding to Figure 3.6.

Case II: m is even.

If m is even, then so is $mn+2$ and hence $\gcd(mn+2, m) \neq 1$. So it must be the case that $\gcd(mn+2, m) = 2$. Thus the winding number is $\frac{m}{2}$, and $\frac{mn+2}{2}$ vertices are covered before we reach the vertex we started with. That is, we cover half of the $mn+2$ vertices before we come back to the vertex we started with.

We need to address how to continue labelling the other half of the vertices once we have come back to vertex 1. In this case, we step by $m+1$ from vertex 1 and label this vertex $\frac{mn+2}{2}+1$. Then we continue stepping by m for the rest of the labelling procedure.

There is one last step to completing the labelling when m is even. This step may seem ad hoc, but is necessary in order for the corresponding dot diagram to have strictly increasing vertex labelling as we move from left to right.

Step by m from vertex $mn+2$ an additional $n-2$ times, increasing the vertex label by 1 each step. This means that there are $n-2$ vertices with

two labels. That is, the vertex labelled $\frac{mn+2}{2}+i$ will be labelled $mn+2+i$ as well, for $1 \leq i \leq n-1$. We use the lower vertex label in diagonals containing vertices 1 up to $n-2$, and use the higher vertex label otherwise. Refer to Figure 3.8 for the case where $m = 2$ and $n = 4$. The corresponding dot diagram can be seen in Figure 3.9.

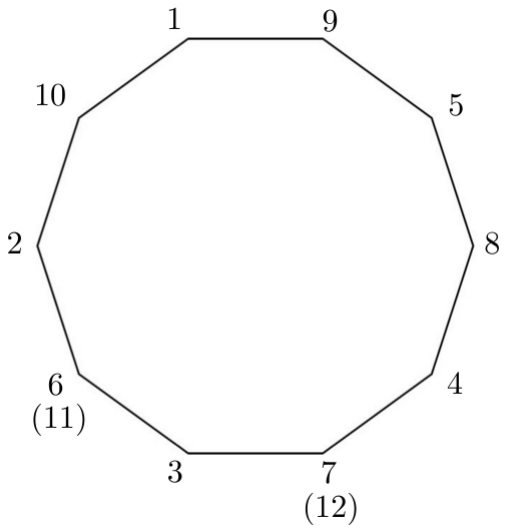

Figure 3.8: Labelling vertices of the 10-gon using the rule described above. For vertices with two labels, the higher label is indicated in brackets.

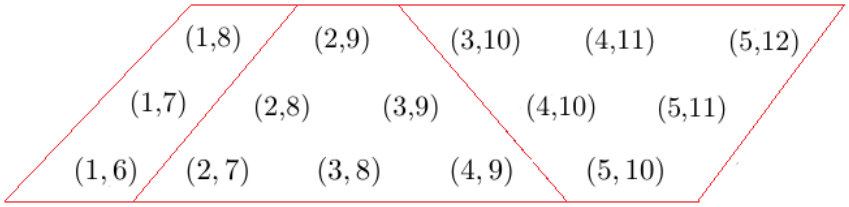

Figure 3.9: The corresponding dot diagram.

3.3 Rotation order on $(m+2)$-angulations

When we label the vertices of an $(mn+2)$-gon using the procedure mentioned in the previous section, we come to a nice description of the rotation order.

Suppose we have two angulations A and B. Then $A \lessdot_r B$ if B is obtained from A by rotating a single diagonal clockwise by one step such that the vertex labelling increases. See Figure 3.10 for an update of Figure 3.2 obtained by using the new vertex labelling.

In Chapter 1, we described the cover relations on the Tamari lattices by flipping a diagonal in a triangulation and moving up in the lattice if the new diagonal has a higher vertex labelling. It is clear that the partial order on the Tamari lattices is just a special case of the rotation order on the m-Cambrian lattices when $m = 1$.

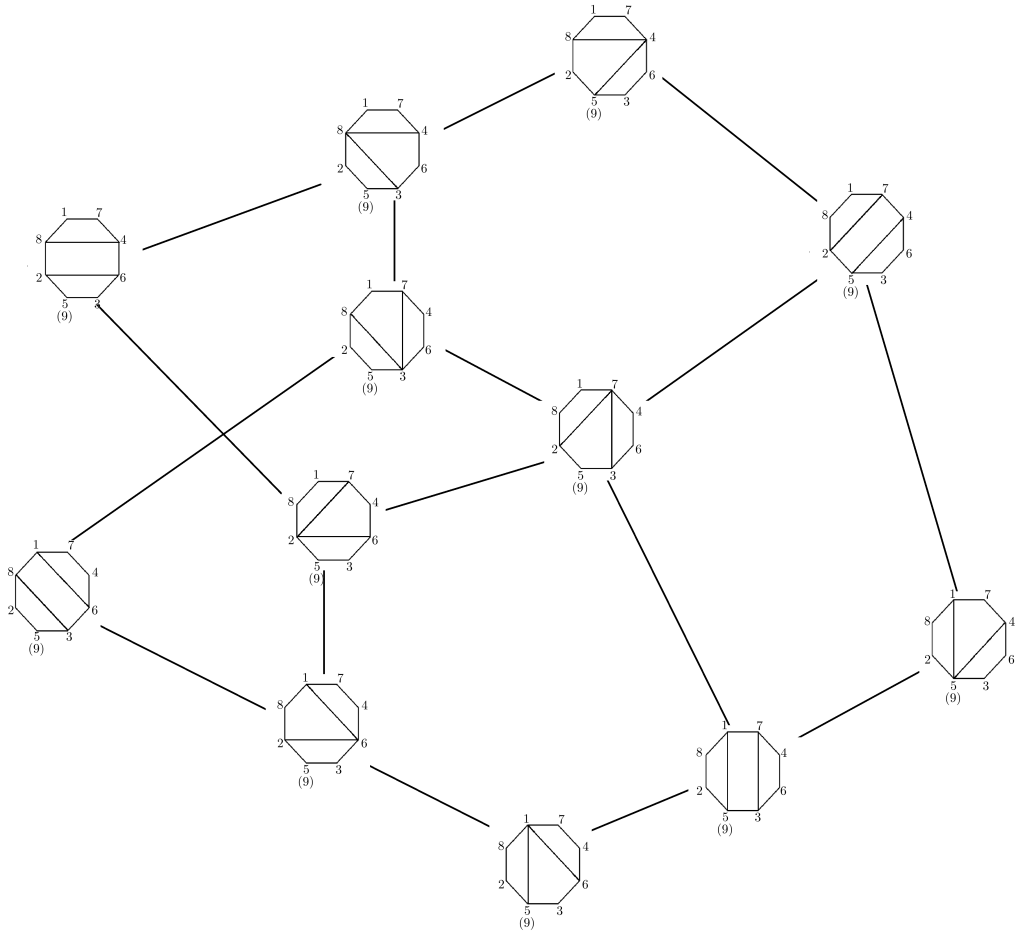

Figure 3.10: We move up in the lattice by rotating a diagonal to a diagonal with higher vertex labelling.

3.4 The second partial order: inclusion order

Given two angulations A and B, we can say that $A \leq_r B$ if there is a sequence of diagonal rotations from A to B such that the vertex labelling is increasing at each step. This is great in theory, but it is not at all obvious whether or not such a sequence exists just from looking at A and B. The second

partial order we will discuss, inclusion order, gives us a better handle on this situation. That is, just looking at A and B will allow us to answer whether or not $A \leq_i B$ (where "$\leq_i$" denotes inclusion order). First, let us make a few observations regarding the movement of shaded dots in dot diagrams.

3.4.1 Right diamonds in dot diagrams

If diagonals (a, d) and (c, b) are present in A and there are no diagonals in A of the form (a, y) or (x, b) such that $b < y < d$ and $a < x < c$, then we know that diagonal (a, b) must flip to (c, d). It is possible that (a, d) and (c, b) are not actually diagonals in the angulation, but are edges of the polygon. These edges are realized as the first row of dots lying above and below the dot diagram (recall Figure 2.7).

The extreme cases for the positions of (a, d) and (c, b) are seen in Figure 3.11, where the dots corresponding to the edges of the polygon are shaded blue. Since (a, d) and (c, b) can independently occupy positions between each extreme in their respective strips, we have all possible dots that (a, b) can flip to contained in the region indicated in Figure 3.12. We call this region the *right diamond* of (a, b). Figure 3.13 illustrates the right diamonds corresponding to dots $(1, 8)$ and $(5, 11)$.

We sometimes are interested in the diamond obtained by moving the right diamond rightward n columns and then reflecting in the horizontal bisector of the diagram. For this reason it is sometimes necessary to refer to the right diamond of (a, b) as the *primary right diamond* of (a, b), its first

rightward glide reflection as the *secondary right diamond* of (a, b), and so on.

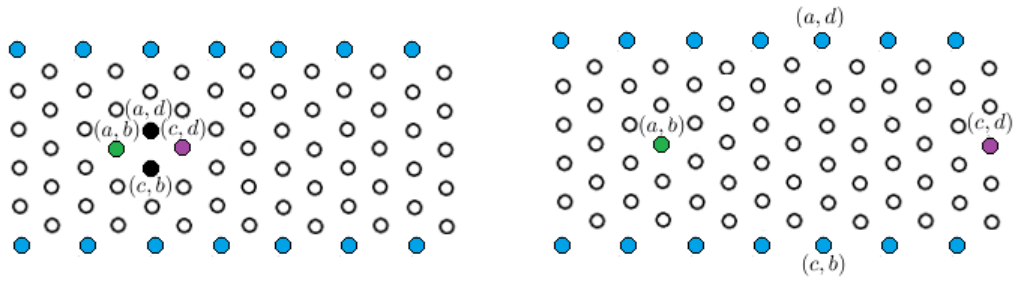

Figure 3.11: The closest (left) and farthest (right) a dot can move in a single flip. The dots of A are shaded green and black, and the dots of B are shaded purple and black.

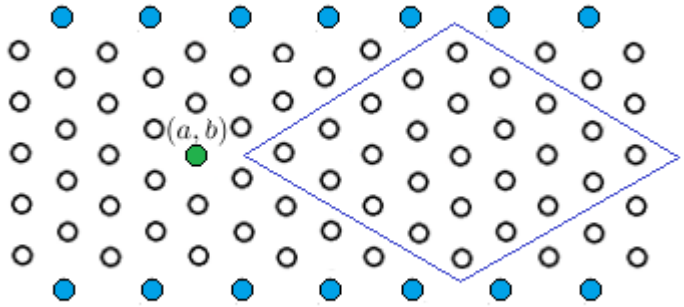

Figure 3.12: The primary right diamond of (a, b) contains all dots that (a, b) can move to in a single flip.

By observing Figure 3.14, we can see that if (a, b) rotates to some diagonal (c, d), then (c, d) must intersect (a, b) somewhere in the interior of the $(mn + 2)$-gon. Since (a, b) is an edge of two $(m + 2)$-gons inside the $(mn + 2)$-gon, removing it leaves us with a $(2m + 2)$-gon. If (c, d) does not

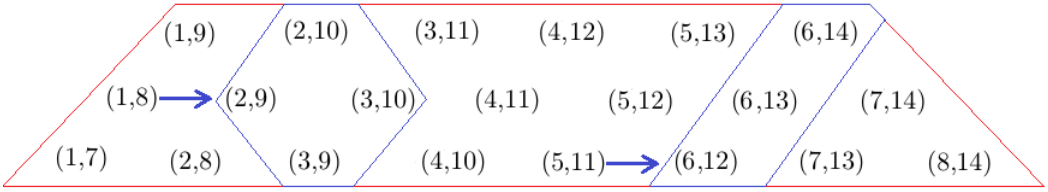

Figure 3.13: The primary right diamonds corresponding to the dots $(1, 8)$ and $(5, 11)$.

intersect (a, b), then it lies either above or below (a, b) in Figure 3.14. In either case we would not be left with two $(m+2)$-gons, and hence this would not be an $(m + 2)$-angulation of the $(mn + 2)$-gon. So if (a, b) rotates to (c, d), then the two diagonals intersect at some point inside the $(mn + 2)$-gon. Furthermore, any clockwise rotation of (c, d) must intersect (a, b) as well.

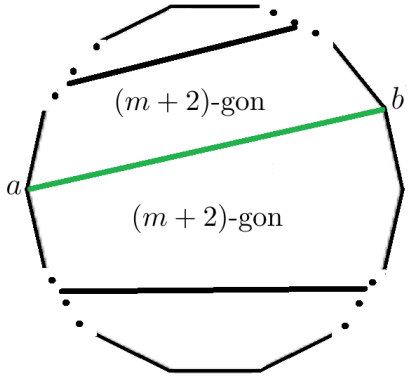

Figure 3.14: Any diagonal that (a, b) rotates to must intersect (a, b) somewhere in the interior of the $(mn + 2)$-gon.

Let us translate this back to dot diagrams and consider all possible

dots that (a, b) can flip to. The above observation says that if the dot (a, b) is shaded in the dot diagram, then none of the dots in its right diamonds can be shaded. See Figure 3.15 for the angulation picture corresponding to Figure 3.13.

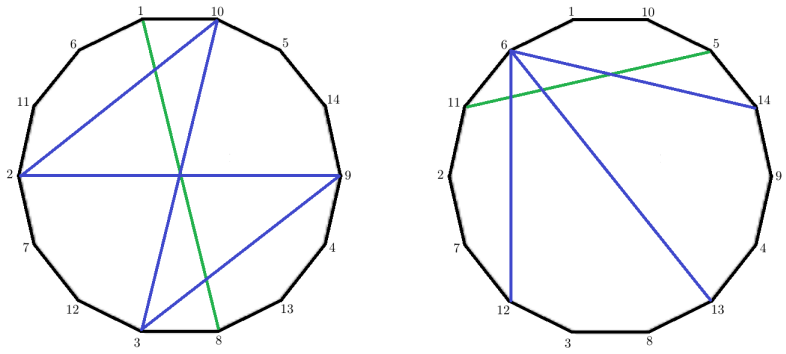

Figure 3.15: Corresponding angulation picture for Figure 3.13

We have yet to show that rotating a diagonal clockwise by one step in the angulation corresponds to moving a black dot rightward to the next legal position in the dot diagram. The following lemma will show that this is in fact the case.

Lemma 3.4.1. *Rotating a diagonal clockwise by one step in an angulation A translates to moving the corresponding black dot rightward to its next legal position in the dot diagram for A.*

Proof. Consider rotating a diagonal (a, b) clockwise by one step in some angulation A. We will split this process into two steps: first we remove the diagonal (a, b) from A, then we replace it with the diagonal (c, d). The

diagonal (a, b) is one of the $m + 1$ possible diagonals of the $(2m + 2)$-gon obtained by its removal from A.

Let's assume that this rotation corresponds to moving the black dot (a, b) to the right to (c, d) (refer back to Figure 3.11). What we need to show is that (c, d) is actually the next legal position to the right of the black dot (a, b). We have seen that the farthest a black dot can move to the right in a single flip is to the rightmost dot in its primary right diamond, i.e., the black dot moves to the right by a full glide reflection.

Recall that a dot diagram consists of a single strip of $n-1$ dots on the left followed by m copies of $\binom{n}{2}$ dots, where the $(i+1)^{st}$ copy is obtained by a glide reflection of the i^{th} copy.

Suppose that in the dot diagram, the black dot (a, b) is found in the i^{th} copy of $\binom{n}{2}$ dots. By rotating (a, b) clockwise in A, we are moving it to the right in the dot diagram no further than a full glide reflection. So (c, d) is no further right within the $(i + 1)^{st}$ copy than (a, b) is within the i^{th} copy. We then rotate (c, d) clockwise by one step and hence move it to the right in the dot diagram no further than a full glide reflection.

By repeating this process, we have at least $m-i+1$ legal positions accounted for before we reach the right end of the dot diagram. We could have rotated (a, b) counterclockwise and hence moved it to the left in the dot diagram no further than a full glide reflection. We can do this at least $i - 1$ times before we reach the left end of the diagram. So we have at least m legal positions accounted for in the dot diagram. However, there are clearly

$m+1$ possible diagonals and hence we have one legal position left to account for.

We know where this last position is in the dot diagram, since we know the labelling of the missing diagonal in the $(2m+2)$-gon. Let's call this missing diagonal (x, y). We can go through the same process of rotating (x, y) and moving the black dot through its legal positions. However, these legal positions must be distinct from the legal positions for (a, b), otherwise we would have picked up (x, y) when finding the legal positions for (a, b). So now we have $2m$ legal positions for diagonals in a $(2m+2)$-gon that only has $m+1$ possible diagonals. Thus we have found a contradiction, and (c, d) is in fact the next legal position to the right of (a, b). □

3.4.2 Left diamonds and the inclusion order

We call the diamond containing (a, b) as its rightmost dot the *left diamond* of (a, b). We interest ourselves as well with the leftward glide reflections of this diamond. The glide reflections are of the same type mentioned in Chapter 2. Here, we move the diamond to the left by n columns and then reflect in the horizontal bisector of the diagram. For this reason it is sometimes necessary to refer to the left diamond of (a, b) as the *primary left diamond* of (a, b), its first leftward glide reflection as the *secondary left diamond* of (a, b), and so on.

We colour a dot red if it is contained in one of the left diamonds for a black dot (a, b), as illustrated in Figure 3.16. The set of red dots generated

by the black dot (a, b) is denoted by $\mathrm{Red}[(a, b)]$. Note that by definition, every black dot is a red dot as well. In our illustrations we will not draw the black dots red, so that we may distinguish between them.

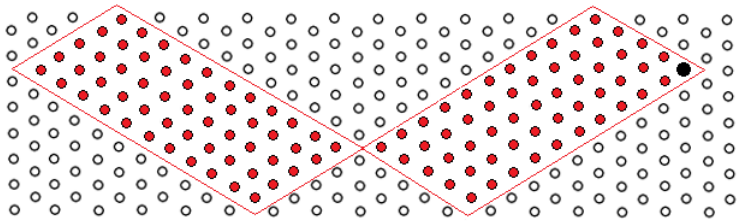

Figure 3.16: The primary and secondary left diamonds for a black dot in some dot diagram.

We are interested in the set of all red dots $\mathrm{Red}[A]$ for a dot diagram A (we will refer to the corresponding angulation as A as well). So we find $\mathrm{Red}[(x, y)]$ for all black dots (x, y) in A and get

$$\mathrm{Red}[A] = \bigcup_{(x,y) \text{ black}} \mathrm{Red}[(x, y)].$$

Then the inclusion order can be described as follows. For two angulations A and B, we write $A \leq_i B$ if $\mathrm{Red}[A] \subseteq \mathrm{Red}[B]$.

This brings us to the main result of the thesis: the two orders we have been discussing are equivalent.

As mentioned at the beginning of this section, this order gives us an easier way to compare two angulations A and B in $\mathrm{Cam}_n^{(m)}$. We simply find the set of red dots in the dot diagram corresponding to A, then do the same for B, and compare one set to the other. This is more efficient than

comparing them with rotation order, where we need to determine whether or not there exists a sequence of diagonal rotations from A to B.

See Figures 3.17, 3.18, and 3.19 for examples of the inclusion order on $\mathrm{Cam}_n^{(m)}$. These are identical to the $\mathrm{Cam}_n^{(m)}$ in Figures 3.1, 3.4, and 3.5 generated using rotation order.

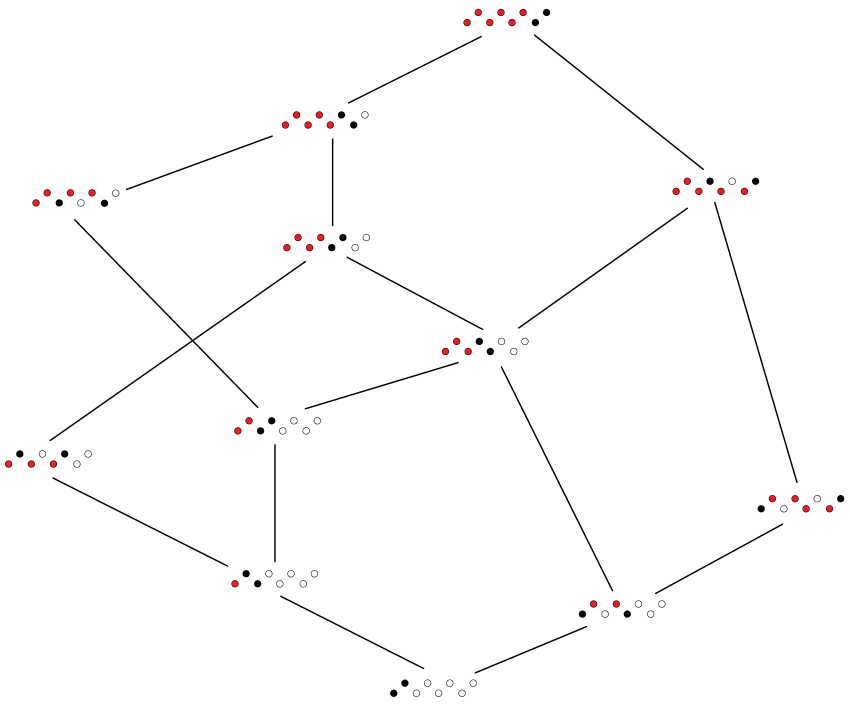

Figure 3.17: Rotation and inclusion order both generate $\mathrm{Cam}_3^{(2)}$.

Before we proceed with a proof of the main result, we will need to convince ourselves of a few facts.

Lemma 3.4.2. *If $A \lessdot_r B$, then $Red[A] \neq Red[B]$.*

Proof. Suppose the black dot (a, b) in A flips to the black dot (c, d) in B.

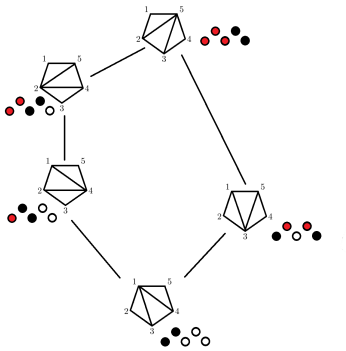

Figure 3.18: Rotation and inclusion order both generate $\mathrm{Cam}_3^{(1)} = T_3$.

Since (a, b) is a black dot in A, we know that none of the dots contained in the right diamonds of (a, b) are black dots of A.

Let us consider the set of dots which generate $(a+1, b+1)$ as a red dot. These are the dots either contained in the diamond with $(a+1, b+1)$ as its leftmost dot, or else contained in one of the rightward glide reflections of this diamond. But these diamonds are exactly the right diamonds of (a, b), and hence there are no black dots in A generating $(a+1, b+1)$ as a red dot. Since (a, b) flips to (c, d), we have that (c, d) is in the primary right diamond for (a, b) and hence generates $(a + 1, b + 1)$ as a red dot. So we have that $(a+1, b+1) \notin \mathrm{Red}[A]$ and $(a+1, b+1) \in \mathrm{Red}[B]$. Thus $\mathrm{Red}[A] \neq \mathrm{Red}[B]$. $\square$

We are now ready to prove the first direction of the main result. We will show that if an angulation A flips to an angulation B then the red dots in the dot diagram for A are a subset of the red dots in the dot diagram for B.

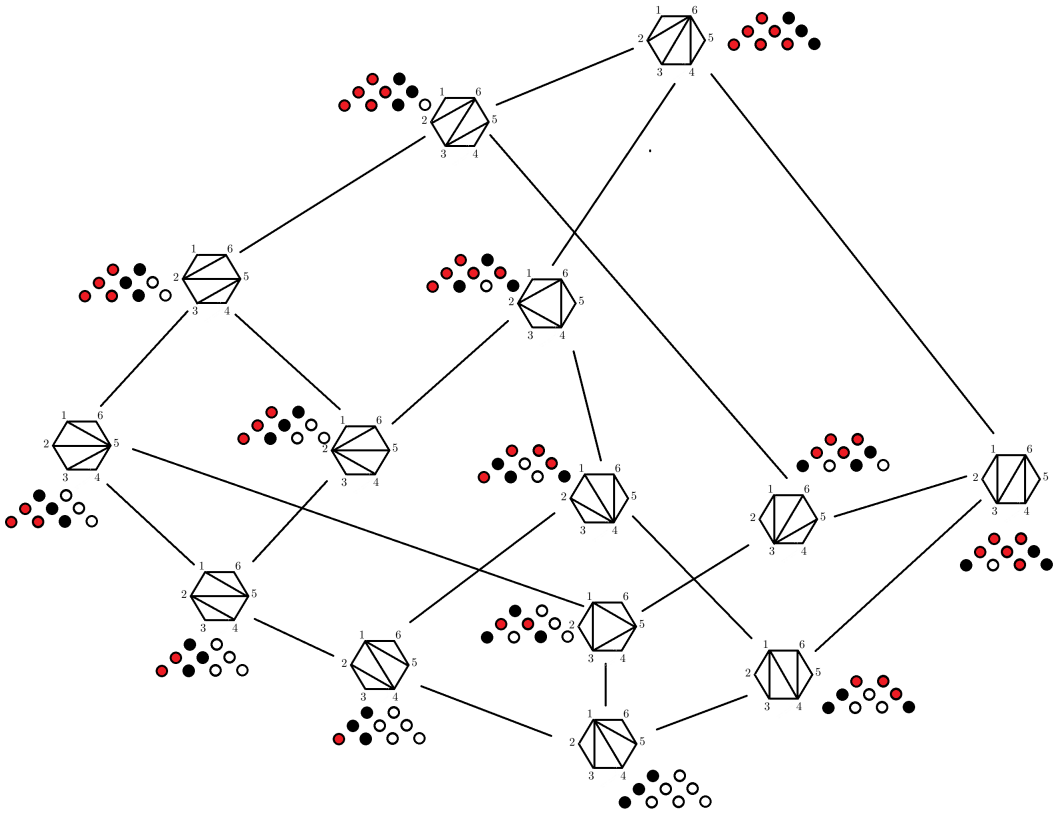

Figure 3.19: Rotation and inclusion order both generate $\mathrm{Cam}_4^{(1)} = T_4$.

Lemma 3.4.3. *Given two angulations A and B, if $A \leq_r B$ then $A \leq_i B$.*

Proof. Suppose that $A \lessdot_r B$. From Lemma 3.4.2, we have that $\mathrm{Red}[A] \neq \mathrm{Red}[B]$. To prove that $\mathrm{Red}[A] \subset \mathrm{Red}[B]$, we are going to show that $\mathrm{Red}[(a,b)] \subset \mathrm{Red}[(a,d)] \cup \mathrm{Red}[(c,b)] \cup \mathrm{Red}[(c,d)]$. Suppose that in the dot diagram, the diagonals (a,b), (c,d), (a,d), and (c,b) are found in rows i, j, k, and l respectively. Then we can explicitly write the numbers which index the boundary edges of the primary left diamonds for these diagonals (see Figure 3.20 for

the primary left diamond of (a, b)).

To show that the red dots generated by (a, b) are a subset of the red dots generated by the other three diagonals of interest, we only need to show that the primary left diamond for (a, b) is covered by the diamonds (primary or otherwise) generated by the other diagonals.

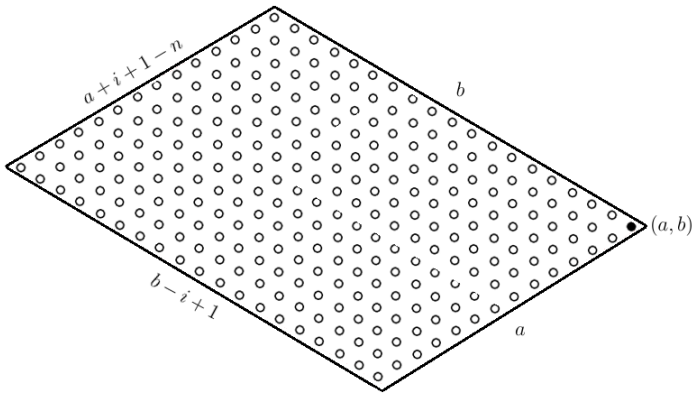

Figure 3.20: The primary left diamond for (a, b).

A sketch for $n = 33$, $i = 19$, $j = 14$, $k = 26$, $l = 7$ can be seen in Figure 3.21.

In Figure 3.22, we can see that if the primary left diamond for (a, b) is the union of disjoint pieces, say X, Y, Z, and W, then X is covered by the primary left diamond for (c, b), Z is covered by the primary left diamond for (a, d), Y is covered by the primary left diamonds for (c, b), (c, d), and (a, d), and W is covered by the secondary left diamond for (c, d).

We will now show algebraically that the coverings described above do in fact hold, by showing how some of the boundary edges of the primary left diamonds coincide. First note that we have

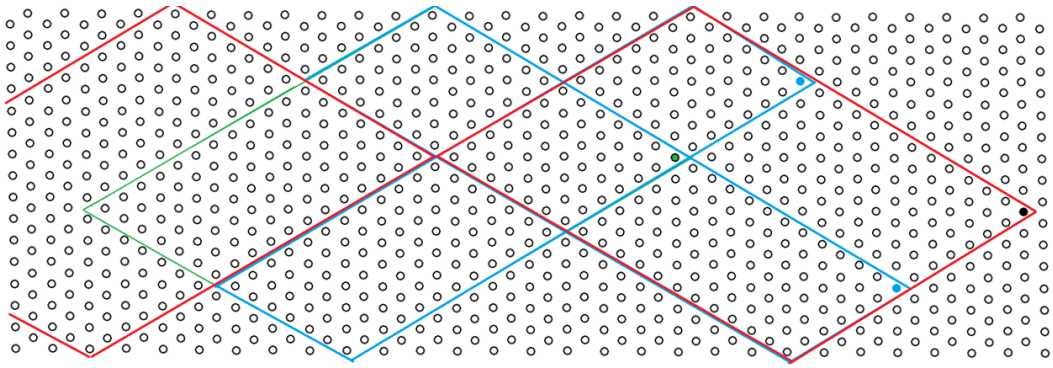

Figure 3.21: The red dots generated by (a, b) are a subset of the red dots generated by (c, d), (a, d), and (c, b).

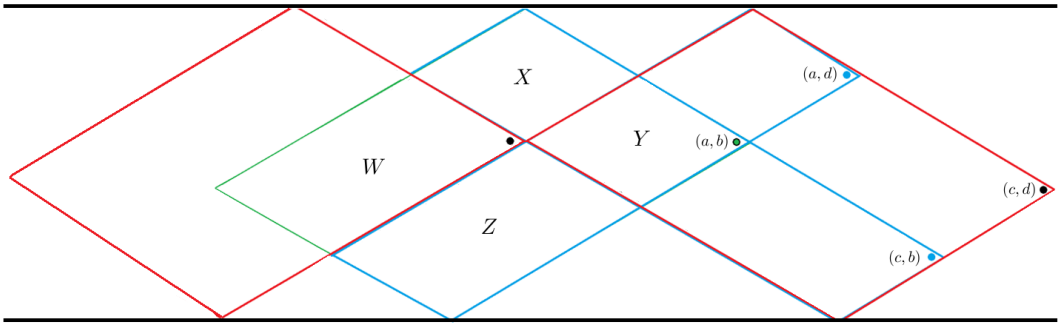

Figure 3.22: The dots have been removed for ease of viewing.

$$k = i + (d - b) = j + (c - a),$$

and

$$l = i - (c - a) = j - (d - b).$$

So

$$\begin{aligned} d - k + 1 &= d - (i + d - b) + 1 \\ &= b - i + 1, \end{aligned}$$

$$\begin{aligned} b - l + 1 &= b - (j - (d - b)) + 1 \\ &= d - j + 1, \end{aligned}$$

$$\begin{aligned} a + k + 1 - n &= a + (j + c - a) + 1 - n \\ &= c + j + 1 - n, \end{aligned}$$

and

$$\begin{aligned} c + l + 1 - n &= c + (i - (c - a)) + 1 - n \\ &= a + i + 1 - n. \end{aligned}$$

Since (c, d) is located in row j, and there are $n - 1$ rows in total, its leftward glide reflection is located in row $n - j$. From the edges of the primary left diamonds for (a, d) and (c, b), we are able to express the leftward glide reflection of (c, d) (i.e., the rightmost dot in the secondary left diamond for (c, d)) as $(a + k - n, b - l)$.

So the bottom-right edge of the primary left diamond for $(a + k - n, b - l)$ is indexed by $a + k - n$, and the top-right edge by $b - l$. Recall

that with the new method of labelling vertices, we get dot diagrams with increasing vertex labelling as we move from left to right. So to show that this diamond covers W in Figure 3.22, we need to show that the top-left edge is indexed by a number no greater than $a + i + 1 - n$, and the bottom-left by a number no greater than $b - i + 1$.

The top-left edge is indexed by

$$\begin{aligned} a + k - n + (n - j) + 1 - n &= a + (k - j) + 1 - n \\ &= a + (c - a) + 1 - n \\ &= c + 1 - n \\ &\leq c + l + 1 - n \\ &= a + i + 1 - n, \end{aligned}$$

and the bottom-left edge is indexed by

$$\begin{aligned} b - l - (n - j) + 1 &= b + (j - l) - n + 1 \\ &= b + (d - b) - n + 1 \\ &= d - n + 1 \\ &\leq d - k + 1 \\ &= b - i + 1. \end{aligned}$$

Hence, we have shown that if $A \lessdot_r B$, then $\mathrm{Red}[A] \subset \mathrm{Red}[B]$. In

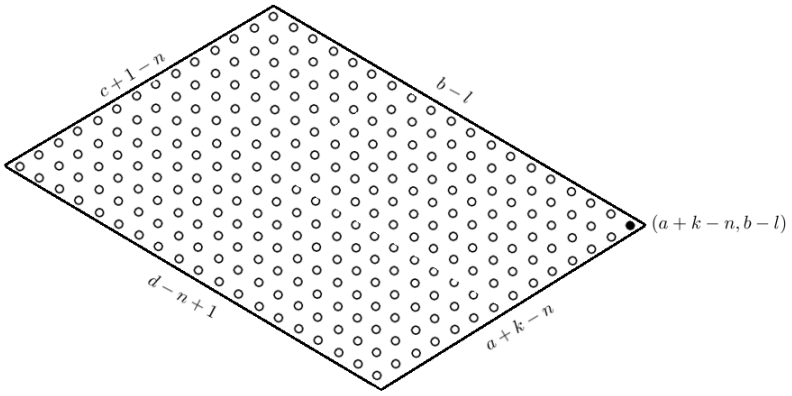

Figure 3.23: The secondary diamond containing red dots generated by (c, d) cover the remaining red dots in the primary left diamond generated by (a, b).

particular, we have shown that when flipping from A to B, we only add red dots in the region Y, and at least add $(a+1, b+1)$ as a red dot (Lemma 3.4.2). It follows from the transitive property of set inclusion that if $A \leq_r B$, then $\text{Red}[A] \subseteq \text{Red}[B]$ and hence $A \leq_i B$. □

We must now establish a few more facts before we can prove the second direction of the main result.

Lemma 3.4.4. *There is a unique minimal element of* $\leq_r$.

Proof. We can observe this fact most readily by looking directly at diagonals in an angulation. If not all the diagonals are connected to vertex 1, then there is at least one diagonal that can be rotated counterclockwise to take it downwards to 1. Furthermore, the unique minimal element of $\leq_r$ is the angulation where all diagonals are attached to vertex 1. □

Corollary 3.4.1. *There is a unique minimal element of* $\leq_i$.

Proof. This follows immediately from Lemmas 3.4.4 and 3.4.3. □

Lemma 3.4.5. *Given two angulations A and B with $A \leq_i B$, let (p, q) be the rightmost black dot of B which is not a black dot of A. Then it is possible to flip (p, q) to the left in the dot diagram for B.*

Proof. Instead of thinking of the dot diagram as a loop, let us think of it as a half-infinite strip by letting it continue infinitely to the left. We also extend the definition of red dots to include dots on the half-infinite strip, by adding infinitely many left diamonds.

Let T be the unique minimal element of $\leq_i$. Then for any $(m+2)$-angulation A, we have that $T \leq_i A$, so $\mathrm{Red}[T] \subseteq \mathrm{Red}[A]$. $\mathrm{Red}[T]$ includes all the virtual dots, as well as the first strip of the regular dots. Thus $\mathrm{Red}[A]$ includes all of these dots as well.

Let (p, q) be the rightmost black dot of B which is not a black dot of A, where $A \leq_i B$. We want to show that it is possible to flip (p, q) to the left. We can always flip a dot to the left in the half-infinite strip we have constructed. Simply do a flip to the left using the dot diagram rules. Suppose (p, q) flips to the left to (a, b), where (a, b) might be either a regular dot in the dot diagram, or else one of the virtual dots we added. We want to argue that (a, b) is a regular dot in the dot diagram, not a virtual dot. We know that $(a + 1, b + 1)$ is not red in A (see proof of Lemma 3.4.2). Since $(a + 1, b + 1)$ is not red in A, it is to the right of the first strip of real dots, and hence (a, b) is also a regular dot. Thus, we can flip (p, q) to the left in the regular dot diagram for B. □

In order to prove the second direction of the main result, we will show inductively that if the red dots of A are a subset of the red dots of B, then there exists a sequence of diagonal rotations from A to B.

Theorem 3.4.1. *Given two angulations A and B, $A \leq_r B$ if and only if $A \leq_i B$.*

Proof. We have already proved the first direction in Lemma 3.4.3. Now we must show that if $A \leq_i B$ then $A \leq_r B$. We will show that if $\mathrm{Red}[A] \subset \mathrm{Red}[B]$, then B can be obtained from A via a sequence of diagonal rotations.

Suppose that we have two angulations A and B such that $\mathrm{Red}[A] \subset \mathrm{Red}[B]$. If we can find an angulation $C_1 \lessdot_r B$ such that $\mathrm{Red}[A] \subset \mathrm{Red}[C_1]$, then inductively we can find a sequence of C_i such that $A \lessdot_r C_p \lessdot_r C_{p-1} \lessdot_r \cdots \lessdot_r C_2 \lessdot_r C_1 \lessdot_r B$.

Let us work in a setting similar to the beginning of the proof of Lemma 3.4.3, except now A is not necessarily covered by B. Suppose that (c, d) is the rightmost black dot of B which is not a black dot of A. Using Lemma 3.4.5, we can flip this dot to the left to position (a, b), and call this new angulation C_1. We can see that the dots (a, d) and (c, b) must be present in both B and C_1.

From Lemma 3.4.3, we have that since C_1 flips to B, then $\mathrm{Red}[C_1] \subset \mathrm{Red}[B]$. We now need to show that $\mathrm{Red}[A] \subset \mathrm{Red}[C_1]$. This will be accomplished by showing that the only red dots we lose when moving from B down to C_1 are the red dots in the primary left diamond for (c, d) which are not

generated by any other dots in B. Furthermore, we will see that these dots are not red dots of A.

Let's consider cutting the primary left diamond for (c, d) into four sections: X, Z, and W which are each contained in some primary left diamond for one of the other three black dots, and Y which is not. We need to show that the secondary left diamond for (c, d) is covered by left diamonds for the other three black dots of interest. Since X, Z, and W are each contained in primary left diamonds for the three dots, their leftward glide reflections, X', Z', and W' are contained in the corresponding secondary left diamonds for these dots. From Figure 3.24, we can see that Y' is entirely contained in the primary left diamond for (a, b). So the only red dots that are lost are those in section Y which are generated by (c, d) and not by any other black dot in B.

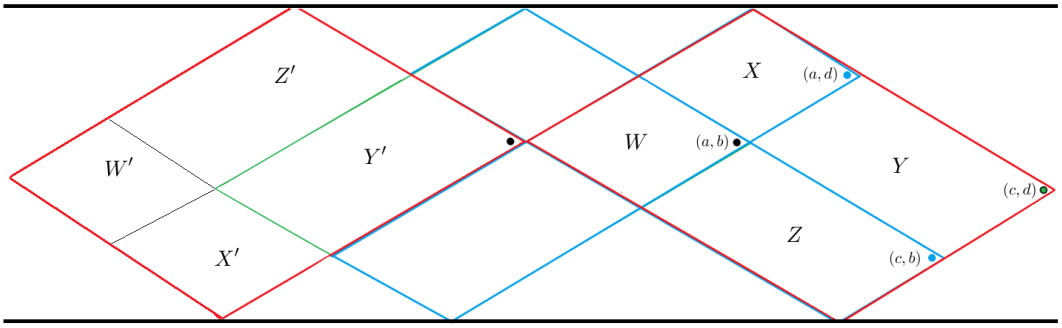

Figure 3.24: Y' is contained in the primary left diamond for (a, b).

Now we must show that the red dots that are lost are not red dots of A. We will assume that there is a red dot of A that is not a red dot of C_1 in section Y and look for a contradiction.

Suppose that $(x, y) \in \text{Red}[A] \cap \text{Red}[B]$ and $(x, y) \notin \text{Red}[C_1]$ such that (x, y) is found in section Y (see Figure 3.25). So (x, y) is lost when moving from B to C_1, and hence is a red dot of B which is in a left diamond for (c, d) and not in a left diamond for any other black dot in B. Since $(x, y) \in \text{Red}[A]$, there must be a black dot (e, f) in A generating a left diamond covering (x, y). We must consider three possible cases for the position of (e, f) in the dot diagram for A.

For the first case, suppose that (e, f) is found to the right of (c, d) so that (c, d) and $(c + 1, d + 1)$ are both contained in some left diamond for (e, f). But we know (from the proof of Lemma 3.4.2) that $(c + 1, d + 1)$ is not a red dot of B. This contradicts the fact that $\text{Red}[A] \subset \text{Red}[B]$.

For the second case, suppose that (e, f) is positioned outside of the region Y and does not contain $(c + 1, d + 1)$ in one of its left diamonds (coloured purple in Figure 3.25). We have that $\text{Red}[A] \subset \text{Red}[B]$ so all other red dots in the left diamond for (e, f) must be covered by black dots in B. In particular, there must be a black dot of B which generates a left diamond covering $(x, d+1)$ but not covering (x, y). The set of black dots which produce left diamonds covering (x, y) is simply the diamond with (x, y) as its leftmost dot (coloured green). Likewise for $(x, d + 1)$ (coloured red).

From the previous subsection, we have seen that the right diamonds of (c, d) consist of diagonals which cross the diagonal (c, d) (primary right diamond shaded grey). Hence, the dots in this diamond are prohibited from being in B due to the presence of (c, d) in B. From Figure 3.25, we can see

that if a black dot in B generates a left diamond covering $(x, d+1)$ but not covering (x, y), then it must either come from this prohibited region (shaded yellow), or else come from a rightward glide reflection of this yellow region. In either case, we find a contradiction since (c, d) is a black dot of B.

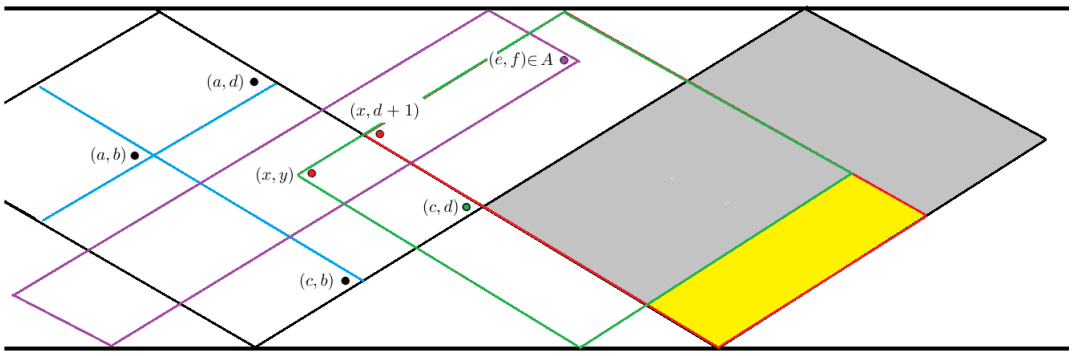

Figure 3.25: The only black dots that cover $(x, d+1)$ but not (x, y) are restricted from being in B due to the presence of (c, d).

For the final case, suppose that (e, f) is positioned inside the region Y. Using a similar argument to the second case, there must be a black dot of B which generates a left diamond covering $(x, d-j)$ (for (c, d) located in row j) but not covering (x, y). From Figure 3.26, we can see that if these black dots are contained in the primary yellow shaded region, then they contain (c, d) in their primary right diamond. If they are contained in a rightward glide reflection of the primary yellow shaded region, then all but one strip are in the right diamond for (c, d). So the only black dots of B that are not immediately ruled out are in the yellow strip just to the left of the right diamond for (c, d). We will show that if $(x, d-j)$ is to be covered by one of these black dots, then there is another red dot of A which can't be a red dot

of B.

If there is a black dot of B in the yellow strip just to the left of the primary right diamond for (c, d), then it has the form (c, w) where $w > d$. So the black dots in this strip lie to the right of (c, d) and hence are black dots of A by assumption. Then some of the lower dots in the yellow strip are ruled out as they are in the primary right diamond of (e, f), and therefore cannot be in A. Let (c, z) be the lowest dot in the yellow strip that is not in the primary right diamond for (e, f). Note that the primary left diamond for (e, f) generates red dots in the x strip from $(x, d-j)$ down to the bottom-left edge of the diamond. The dot (c, z) is chosen so that out of all dots in the yellow strip, its left diamonds cover the most of this section of the x strip. In fact, the only red dot in this section of the x strip that is generated by (e, f) but not by (c, z) is the dot at the bottom-left edge. Let's call this dot (x, p). If we consider the set of all black dots that generate (x, p) as a red dot but do not generate (x, y) as a red dot, we find a contradiction. In one case the black dot lies to the right of (c, d), so that it is a black dot of A, but also is contained in a right diamond for (e, f). In another case (c, z) is in a right diamond of the black dot. In the final case (e, f) generates the dot just to the right of the black dot as a red dot, which contradicts the fact that $\text{Red}[A] \subset \text{Red}[B]$.

Thus, there are no red dots of A lost when moving from B to C_1.

So we have found a $C_1 \lessdot_r B$ such that $\text{Red}[A] \subset \text{Red}[C_1]$. We can now find $C_2 \lessdot_r C_1$ by moving the rightmost dot of C_1 that is not a dot of

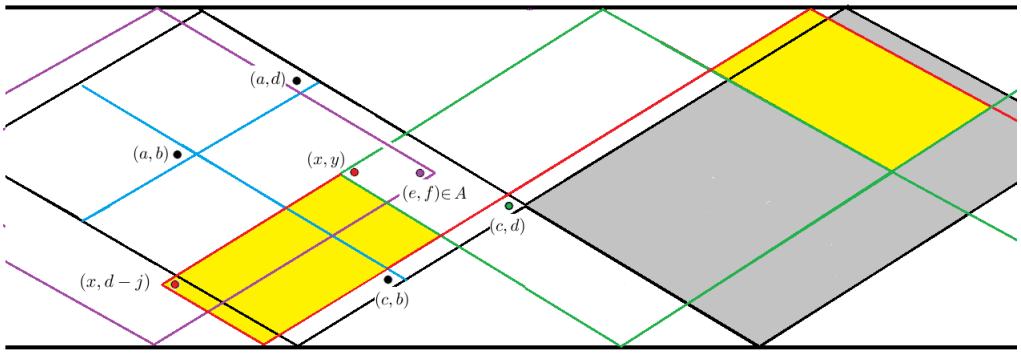

Figure 3.26: The only black dots that cover $(x, d-j)$ but not (x, y) are restricted from being in B due to the presence of (c, d).

A. We can continue this process until we have moved down to A itself. So we have found a sequence of diagonal rotations from A to B, namely the C_i satisfying $A \lessdot_r C_p \lessdot_r C_{p-1} \lessdot_r \cdots \lessdot_r C_2 \lessdot_r C_1 \lessdot_r B$.

Thus, the second direction is proved, and we have $A \leq_r B$ if and only if $A \leq_i B$. □

Chapter 4

Future work

We did not show that the m-Cambrian partial orders defined actually produce a lattice. This is something that I will prove in future work.

4.1 Red dots as diagonals

We have a nice description for the rotation order using the language of diagonals in an $(m+2)$-angulation of an $(mn+2)$-gon. Namely, we rotate a diagonal clockwise one step and move up in the lattice if the vertex labelling increases. Can we have such a natural description for the inclusion order using the language of diagonals in an angulation?

In Figure 4.1, we translate the dot diagrams in Figure 3.17 to the corresponding quadrangulations of an octagon. When we do this translation from dot diagrams to angulations, we can certainly describe the inclusion

order in terms of sets of red diagonals. The problem is that the description is not natural. It is a cumbersome process to see which diagonals we colour red for a given black diagonal. So for inclusion order, it appears that dot diagrams are a much more useful picture to work with.

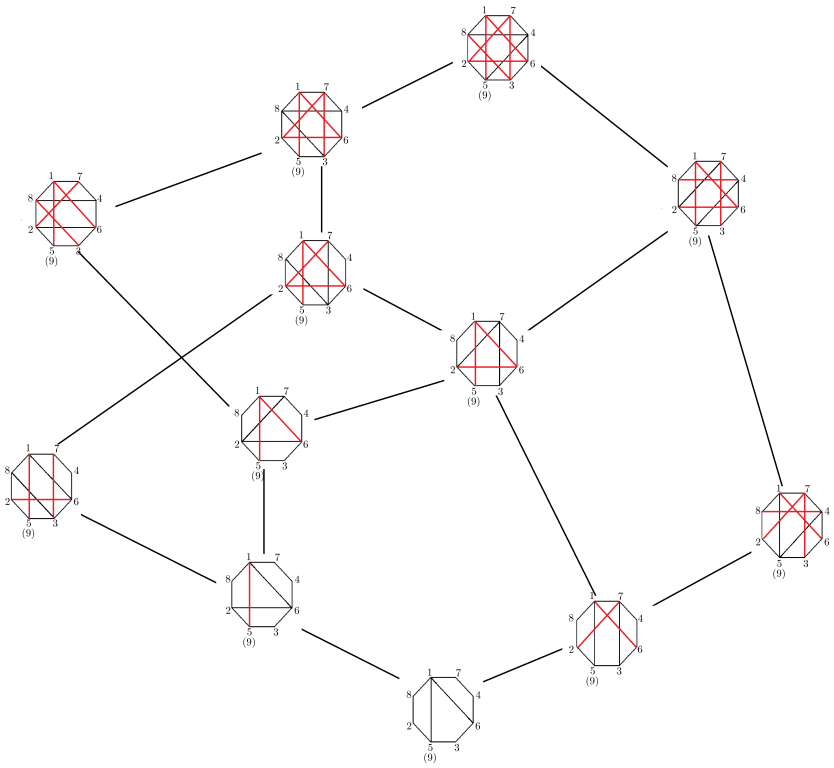

Figure 4.1: Colouring dots in the 2-Cambrian lattice.

One of my goals for future work is to find a more natural description for the inclusion order using the language of angulations.

4.2 Other partial orders

There exist two beautiful descriptions of partial orders on the Tamari lattices: *snug rectangles*, introduced by Hugh Thomas [14], and *submersion sets*, introduced by Edelman and Reiner [6].

Since T_n is just a special case of $\mathrm{Cam}_n^{(m)}$ when $m = 1$, it would be interesting if there were generalizations of each order for $m > 1$. My future work will involve searching for such generalizations.

Bibliography

[1] D. Armstrong, B. Rhoades, and N. Williams, *Rational associahedra and noncrossing partitions*. Submitted, (2013). arXiv: 1305.7286

[2] F. Bergeron and L-F. Preville-Ratelle, *Higher trivariate diagonal harmonics via generalized Tamari posets*, Journal of Combinatorial Theory, 3(3):317341, (2012).

[3] F. Bergeron, *Combinatorics of r-Dyck paths, r-Parking functions, and the r-Tamari lattices*, (2012). arXiv:1202.6269.

[4] O. Bernardi and N. Bonichon, *Catalan intervals and realizers of triangulations*, Journal of Combinatorial Theory, Series A Volume 116, Issue 1, 55-75, (2009).

[5] A. Björner and F. Brenti, *Combinatorics of Coxeter Groups*, Graduate Texts in Math. 231, Springer, New York, (2005).

[6] P. Edelman and V. Reiner, *The higher Stasheff-Tamari posets*, Mathematika 43, 127-154, (1996).

[7] S. Fomin and N. Reading, *Generalized cluster complexes and Coxeter combinatorics*. IMRN 2005:44, 27092757, (2006).

[8] M. Haiman, *Vanishing theorems and character formulas for the Hilbert scheme of points in the plane*, Inventiones Mathematicae 149 No.2, 371-407, (2002).

[9] J.E. Humphreys, *Reflection Groups and Coxeter Groups*, Cambridge University Press, Cambridge, 1990.

[10] N. Reading, *From the Tamari lattice to the Cambrian lattices and beyond*, Chapter from *Associahedra, Tamari Lattices and Related Structures* (2012). arXiv:1109.5105

[11] R. Stanley, *Catalan addendum to Enumerative Combinatorics, Volume 2*, personal website, (2013).

[12] C. Stump, H. Thomas, N. Williams, *Cataland: Why the Fuss?*, (2015). arXiv:1503.00710

[13] D. Tamari, *Monoides preordonnes et chaines de Malcev*, Doctorat es-Sciences Mathematiques These de Mathematique, Paris, (1951).

[14] H. Thomas, *Maps between higher Bruhat orders and higher Stasheff-Tamari posets*, (2002). arXiv:math/0212097

[15] H. Thomas, *Defining an m-cluster category*, (2007). arXiv:math/0607173

[16] G. Ziegler, *Lectures on Polytopes*, Graduate Texts in Mathematics 152, Berlin, New York: Springer-Verlag, (1995).

Curriculum Vitae

Michael Patrick Freeze
University of New Brunswick: Bachelor's of Science September 2008 to May 2012.